

Review of «Landscape response to tectonic deformation and cyclic climate change since ca. 800 ka in the southern Central Andes» - Orr. et al.

General comments:

- **Scientific significance (Good):** the paper discusses the importance of alluvial records in capturing climate variability relative to the length of rivers within an orogenic system, specifically in broken foreland setting. This topic is intriguing because the organization and spatial patterns of alluvial terraces and fans may be indicative of various driving factors, including tectonic activity, climatic changes, and autogenic processes. The results presented in the manuscript add valuable insights into the interpretation of alluvial sequences during the late Pleistocene.
- **Scientific quality (Good):**
 - Methods:
 - The authors have mapped alluvial fans using satellite imagery along with DEMs and have dated these features using Cosmogenic Radionuclide ^{10}Be derived from surface samples and a depth profile. One can regret that the analysis of the surface samples did not also incorporate ^{26}Al , as this dual measurement could have provided a more comprehensive discussion of the laboratory errors or potential sample inheritance issues that might affect the ^{10}Be age estimates.
 - The authors should introduce here how the depth profile provides more reliable results and how to use the results versus the surface exposure age.
 - Are there any erosional rates available for this area? If so, this could impact the CRN ages.
 - Furthermore, the authors distinguish between the ages of the alluvial fans' aggradation and their ages of abandonment. This aspect is quite interesting, but the method by which the abandonment ages were determined remains unclear to me. Although the authors cite earlier studies, it would be beneficial to elaborate on the methodology and clarify the uncertainties associated with these results, as they play a crucial role in the discussions presented in the paper.
 - Eventually, in Figures 6C and 7C, the authors display areas of probable age for the terraces using the Probability Density Functions. Could you remind here the concept?
 - Results: I find the section 4 dedicated to the results, not well adjusted. The section starts with a conclusion of the results comparing two generations of fans (G1 and

G2). This helps to split the description of the results in two subsections dedicated to G1 fans and then G2 fans but it is confusing in the reading as all information and discussion are given at the same time. You have first to show that you are working on alluvial fans, then you date them. I would rewrite the section 4 as follow:

- Section 4.1: a description of the alluvial fans morphology, arrangement (cut and fill, fill-cut, strath), sediment types/size, slope illustrated with pictures (Qf_1 and Qf_5 are not shown on Figure 3) from the field or extracted from satellite images. In this section, it might be good to have a longitudinal incision profile of the alluvial fans versus their nearest stream (height of alluvial fans with regards to the stream bed rock versus distance to the river outlet with significant vertical exaggeration) since you give those values in the text. This could fit in Figure 3.
 - Section 4.2: CRN ages of the surface activity and abandonment of the individual alluvial fans described in 4.1 and discuss potential inheritances/erosional factors.
 - The identification of two generations of fans is either a conclusion to this section 4 (4.3) or part of the discussion.
- Discussion: The discussion presented in the paper is engaging but occasionally difficult to follow, largely due to the absence of visual aids to clarify the various hypotheses being examined. In my view, the paper's findings predominantly indicate a renewed phase of incision after 750 ka, which the authors attribute to the shift in the duration of glacial cycles during the Middle Pleistocene Transition (1.2-0.8 Ma). Additionally, the research points to a depositional hiatus between 500 and 100 ka in the tributaries of the lower Toro Basin, whereas during the same period, alluvial terraces were developing along the Toro River in the upper basin. To explain this spatio-temporal variabilities, the authors work on three hypotheses: (i) tectonic uplift in the upper reaches, (ii) upstream/downstream incision/aggradation feedbacks, (iii) response time to base level variabilities due to climate variabilities.
- The authors favor hypothesis (iii) but the impact of the base level variability in the Lerma Valley at the Toro Basin outlet has been poorly investigated. There is a possibility that autogenic processes or the reorganization of the drainage network may control a sudden drop in base level. Additionally, the contribution of tectonic uplift at the basin's outlet versus the river erosion power, as detailed by Hilley and Strecker (2005), needs consideration. If these two processes sustain a sufficiently elevated base level, the system's response time could be significantly prolonged, which would give predominance to hypothesis (ii).

- The authors dismiss hypothesis (i), yet this requires further clarification since tectonic uplift rates comprise 50 to 80% of the incision rates. Consequently, a question arises as to why tectonic uplift couldn't be responsible for multiple generations of alluvial fans. It would be beneficial for the authors to explain this reasoning in more detail.
- To aid in comprehending the various hypotheses, I recommend including additional figures:
 - A table that succinctly compares the periods of activity and abandonment of the alluvial fans with the ages of the downstream terraces as identified in Tofelde et al. (2017).
 - A composite figure that visually represents the three hypotheses could be particularly helpful. This could take the form of schematic longitudinal profiles extending from the lower Toro Basin to the Lerma Valley, including the downstream tectonic barriers. The figure should illustrate how the longitudinal profile has evolved over time and how these changes correspond to the alluvial records. We should not rule out that all three hypotheses may contribute simultaneously.

One aspect that requires further clarification is the rationale behind the G2 fans reflecting climate periodicity of 20 to 40 kyr, as outlined in section 5.4. While initially introduced as a tentative hypothesis, this conclusion seems to be presented later as a more definitive outcome. Additionally, this premise is based on the constrained age distribution of the G2 fans, which is specified as between 21 and 40 kyr in section 5.1.2. However, there is a discrepancy, as the ages from CRN dating and the derived abandonment ages indicate a narrower span, with differences between terraces typically ranging from 5 to 20 kyr.

To clarify, section 5.1.2 should delve deeper into addressing the uncertainties associated with the ages, which could include potential inheritance effects or erosion impacts. It should also expound upon the aggradation activity duration, the precise timing of terrace abandonment, and how these periods correlate with global climate benchmarks such as Marine Isotope Stages (MIS), which have been utilized for the G1 fans' chronology.

- **Presentation quality (Fair):** as stated above, I would recommend improving or restructuring some sections (results and discussion). I would restructure the section 3 *Methodology* as follow:

3.1 Mapping of the alluvial fans (from the field, satellite imagery and DEM)

3.2 CNR dating

3.2.1 *¹⁰Be surface exposures*

3.2.2 *Depth Profile*

3.3 *Surface abandonment (detail more d'Arcy et al., 2019)*

Also, I would also clarify some figures

- Figure 1: The primary structural elements (thrusts, axes of anticlines/synclines) should be depicted in Figure 1B. This addition would clarify where tectonic uplifts might be anticipated and indicate the locations of active tectonic barriers to rivers. Also, what are the meaning of TRMM2B3, SASM and MPT (pentagon symbols) in the caption? In the section on climate setting or within the figure caption, please specify which glacial records are being referenced. If these records are not addressed in the text, they should be omitted from the figure to avoid confusion.
- Figure 2:
 - The color coding on the geological map (Figure A) could be made clearer—perhaps reducing the transparency would help.
 - It would be useful to include the slope values for the Rio Toro segments and its tributaries in Figure B. These are key geomorphic metrics and would aid in comparing this study with others.
 - The relevance of the knickpoint highlighted in the close-up of Figure B needs clarification. Is the delayed incision due to variability in bedrock or river morphometrics? This point warrants discussion in the text. Additionally, the paper would benefit from a satellite image of the Toro basin, delineating all the alluvial fans and terraces, similar to what is shown in Figure 4 of Hilley and Strecker (2005).
- Figure 3:
 - I would recommend to add a close-up satellite image of the alluvial fans.
 - Add geographical orientations on the sections.
 - Specify in the caption the type of projection on the section (orthogonal, distance?).
- Figure 5: The picture of the transect is too small. It would be worth to make it bigger.
- Figure 6:
 - The CaCO₃ graph in Figure 6A appears to be inconsistent with the age of the G1 fans; thus, it may be unnecessary to include this graph.
 - There does not seem to be any mention of Figure 6B in the text. If this figure isn't utilized, it should be removed to maintain clarity.
 - In Figure 6C, distinct symbols should be used to mark the samples suspected to be affected by erosion or inheritance, as well as those that are stratigraphically inconsistent. Implementing this would better emphasize

the conclusion that the alluvial fans were actively forming between 750 and 500 ka.

- I question the relevance of referencing Marine Isotope Stages (MIS) in this context since the age uncertainties associated with the fans surpass the resolution of MIS periods. Moreover, it does not appear that MIS are mentioned elsewhere in the text.
- Could you specify the meaning of PDF in the caption?
- Figure 7: the ages of 60-65 ka determined for the surface activity and abandonment of the Qf_5-7 seem to correspond with Marine Isotope Stage 4 (MIS4). This connection is noteworthy and should be mentioned.
- Figure 8: Could you provide the ages of the individual alluvial fans generation and terraces in the legend?
- Figure 9: Could you clarify which references pertain to the various boxes and highlight which results are from your own study?

I have added additional comments to the pdf files.

I am sorry for all those detailed comments, but I think that they will help increasing the quality of the manuscript.

Grégoire Messenger



1 Landscape response to tectonic deformation and cyclic climate change since ca. 800 ka
2 in the southern Central Andes

3
4 Elizabeth N. Orr^{1,2*}, Taylor F. Schildgen^{1,3}, Stefanie Tofelde⁴, Hella Wittmann¹ and Ricardo N.
5 Alonso⁵
6

7 1: GFZ German Research Centre for Geosciences, Telegrafenberg, 14473 Potsdam, Germany

8 2: Department of Geography, Durham University, Durham, DH1 3LE, United Kingdom

9 3: Institute for Geosciences, University of Potsdam, Karl-Liebknecht-Str. 24-25, 14476 Potsdam, Germany

10 4: Institute of Geological Sciences, Freie Universität Berlin, 12249 Berlin, Germany

11 5: Facultad de Ciencias Naturales, Universidad Nacional de Salta, Salta, 4400 Argentina

12 *Corresponding author: Elizabeth N. Orr (elizabeth.orr2@durham.ac.uk)

13

14 Abstract

15 Theory suggests that the response time of alluvial channel long-profiles to perturbations in climate is
16 related to the magnitude of the forcing and the length of the system. Shorter systems may record a
17 higher frequency of forcing compared to longer systems. Empirical field evidence that system length
18 plays a role in the climate periodicity preserved within the sedimentary record is, however, sparse. The
19 Toro Basin in the Eastern Cordillera of NW Argentina provides an opportunity to test these theoretical
20 relationships as this single source-to-sink system contains a range of sediment deposits, located at
21 varying distances from the source. A suite of eight alluvial fan deposits is preserved along the western
22 flanks of the Sierra de Pascha. Farther downstream, a flight of cut-and-fill terraces have been linked to
23 eccentricity-driven (100-kyr) climate cycles since ca. 500 ka. We applied cosmogenic radionuclide
24 (¹⁰Be) exposure dating to the fan surfaces to explore (1) how channel responses to external perturbations
25 may or may not propagate downstream, and (2) the differences in landscape response to forcing
26 frequency as a function of channel length. We identified two generations of fan surfaces: the first (G1)
27 records surface activity and abandonment between ca. 800 and 500 ka and the second (G2) within the
28 last 100 kyr. G1 fans record a prolonged phase of net incision, which has been recognised throughout
29 the Central Andes, and was likely triggered by enhanced 100-kyr global glacial cycles following the
30 Mid-Pleistocene Transition. Relative fan surface stability followed, while 100-kyr cut-and-fill cycles
31 occurred downstream, suggesting a disconnect in behaviour between the two channel reaches. G2 fans
32 record higher frequency climate forcing, possibly the result of precessional forcing of climate (ca.
33 21/40-kyr timescales). The lack of a high-frequency signal farther downstream provides field support
34 for theoretical predictions of a filtering of high-frequency climate forcing with increasing channel
35 length. We show that multiple climate periodicities can be preserved within the sedimentary record of
36 a single basin. Differences in the timing of alluvial fan and fluvial terrace development in the Toro
37 Basin appears to be associated with how channel length affects fluvial response times to climate forcing
38 as well as local controls on net incision, such as tectonic deformation.



39 Plain Language Summary

40 Fluvial terraces and alluvial fans in the Toro Basin, NW Argentina record river evolution and global
41 climate cycles over time. Landform dating reveals lower-frequency climate cycles (100-kyr) preserved
42 downstream and higher-frequency cycles (21/40-kyr) upstream, supporting theoretical predications that
43 longer rivers filter out higher-frequency climate signals. This finding improves our understanding of
44 the spatial distribution of sedimentary paleoclimate records within landscapes.

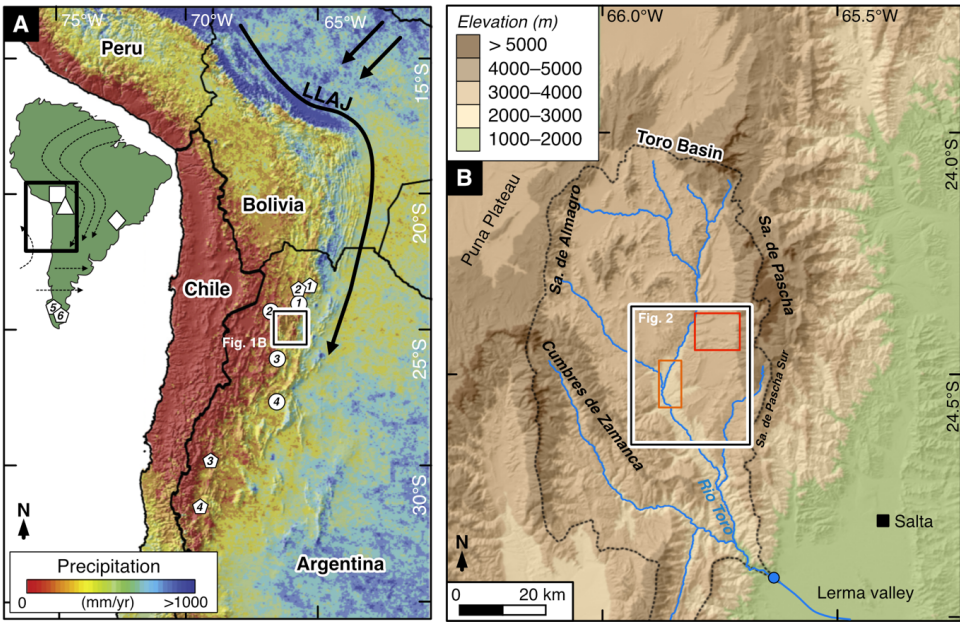
47 1. Introduction

48
49 Fluvial landforms, sediment deposits and the channel form of alluvial systems can be used to reveal
50 landscape response to past environmental change (Castelltort and Van Den Driessche, 2003; Godard et
51 al., 2013; Dey et al., 2016; Romans et al., 2016; Mescolotti et al., 2021). Alluvial channels respond to
52 climate or tectonic driven changes in water discharge, sediment discharge, or base level elevation by
53 adjusting at least one of their characteristics: bed slope, channel width, channel depth, sediment
54 transport rates or grain-size distribution (Mackin 1948; Savi et al., 2020). We can observe this channel
55 adjustment via sediment aggradation or incision events, which modify channel bed elevations (Howard,
56 1982; van den Berg et al., 2008; Wickert and Schildgen, 2019; Tofelde et al., 2019). Fluvial landforms
57 such as terraces and alluvial fans, which develop along these channels because of this aggradation or
58 incision, can provide a useful record of how the alluvial-channel system has evolved over time (Rohais
59 et al., 2012; Armitage et al., 2013; Kober et al., 2013; Counts et al., 2015; Mather et al., 2017; Tofelde
60 et al., 2021).

61
62 Theory suggests that the time required for an alluvial-channel long profile to adjust to a change in
63 climate forcing (response time) varies with the magnitude and type of the forcing (sediment supply
64 versus water supply) and the length of the system; shorter systems respond faster and, hence, may record
65 a higher frequency of forcing compared to longer systems (Paola et al., 1992; Castelltort and Van Den
66 Driessche, 2003; Godard et al., 2013; McNab et al., 2023). The length scale over which periodic forcing
67 delivered at the channel head affects the channel long profile is proportional to the square root of the
68 period of the forcing (Paola et al., 1992), which means that higher frequency forcing is filtered out with
69 distance downstream. Evidence of this relationship is preserved in several sedimentary basins in the
70 Central Andes. Tributary catchments of the Humahuaca Basin (23°S) retain late Quaternary fluvial
71 deposits between 10 and 100 km downstream from the basin headwaters, which record precessional (21
72 kyr) cycles in aggradation and incision (Schildgen et al., 2016). In the Toro Basin (24.5°S), a flight of
73 fluvial cut-and-fill terraces with periodicity of 100-kyr has been linked to eccentricity-driven climate
74 change (Tofelde et al., 2017). These terraces have an upstream channel length of ~60–80 km. Pliocene-



75 Late Pleistocene sediment deposits are preserved ~140–160 km downstream from the headwaters of
76 the Iruya Basin (22°S) of the northern Central Andes and record long eccentricity (400-kyr) cycles
77 (Fisher et al., 2023). Crucially, only a single climate periodicity has been recorded in each these basins
78 to date. To further test this theoretical relationship between climate periodicity and system length, we
79 aim to investigate whether multiple periodicities can be preserved within a single basin, and if this is
80 the case, whether higher frequency climate forcing is only observed in the uppermost reaches of the
81 basin.
82



83
84 **Figure 1.** Overview of the topography, rainfall and moisture transport of the Central Andes. A) TRMM2B31 rainfall map
85 (Bookhagen and Strecker, 2008). Moisture is transported (black arrows) from Atlantic sources during the **SASM** by the Low-
86 Level Andean Jet (LLAJ; Vera et al., 2006). The Toro Basin is outlined by the white-black bordered box. Circle symbols
87 denote regional glacial record locations: (1) Nevado de Chañi (24.0°S, 65.7°W; Martini et al., 2017), (2) Quevar Volcano
88 (24.4°S, 66.8°W; Luna et al., 2018), (3) Sierra de Quilmes (26.2°S, 66.2°W; Zech et al., 2017) and the (4) Sierra de Aconquija
89 (27.2°S, 66.1°W; D’Arcy et al., 2019a). Pentagon symbols denote **MPT** geomorphic record locations: (1) Casa Grande Basin
90 (23°S, 66.5°W; Pingel et al., 2019b), (2) Salinas Grandes Basin (23.5°S, 66°W; Pingel et al., 2019b), (3) Iglesia Basin (30.5°S,
91 69°W; Terrizzano et al., 2017), (4) Calingasta Basin (32°S, 69.5°W; Peri et al., 2022), (5) Río Deseado (47°S, 72°W; Tobal et
92 al., 2021), (6) Río Santa Cruz (50°S, 73°W; Milanez Fernandes, 2023). Inset map of South America indicates Fig. 1A extent
93 and the location of the Lake Titicaca (square symbol; Fritz et al., 2007), Salar de Uyuni (triangle symbol; Baker et al., 2001)
94 and Botuverá Cave (diamond symbol; Wang et al., 2007) paleoenvironmental records. Dashed arrows outline the moisture-
95 bearing low-level airflow patterns for South America which are deflected by the Andean topography. B) Topography of the
96 Toro Basin (ca. 4000 km², 1500–5900 m asl) from TanDEM-X (12-m resolution) elevation data. Basin outlined by dashed
97 black line. Upper basin delineated by white-black bordered rectangle (see Fig. 2). Toro alluvial fans and fluvial terraces
98 outlined by red and orange rectangles, respectively. Basin outlet and start of long profile in Fig. 2 is shown by blue circle. Sa-
99 Sierra.

100
101 Approximately 30 km upstream of the 100-kyr cut-and fill terraces in the Toro Basin is a suite of well-
102 preserved alluvial fan surfaces which extend from tributary catchments that drain the Sierra de Pascha
103 (Fig. 1). There is limited evidence of sediment storage in these tributary catchments en route to the fans.
104 With an upstream channel length of ~10 km, this fan record may capture geomorphic change linked to



a higher frequency climate forcing than the downstream terraces. The Toro Basin alluvial-channel system therefore allows us to explore (1) how channel responses to external perturbations may or may not propagate downstream, and (2) the differences in landscape response to forcing frequency as a function of channel length when comparing the upper basin alluvial fan deposits with the lower basin terrace sequence.

To address these aims, we dated the suite of fan surfaces in the upper Toro Basin using *in situ*-¹⁰Be cosmogenic radionuclide (CRN) dating. We used our new Toro fan chronostratigraphy in conjunction with the fluvial terrace record of Tofelde et al. (2017) to further characterise the evolution of the Toro Basin over the last million years.

2. Regional setting

The Toro Basin (24.5°S) is an intermontane basin in the Eastern Cordillera of NW Argentina, located between the high elevation Puna Plateau to the west and the low elevation Andean foreland to the east (Fig. 1). The mainly gravel-bedded Río Toro flows predominantly south from the low relief upper reaches of the basin with thick successions of preserved sediment, which are the focus of this study (referred to as the upper Toro Basin herein), through a steep bedrock gorge, before draining into the Cabra Corral reservoir in the Lerma valley (Marrett and Strecker 2000; DeCelles et al., 2011). The diffuse shifts in channel steepness along its course are characteristic of arid, tectonically active landscapes with mechanically strong basement rocks (Fig. 2B, C) (Bernard et al., 2019, Zondervan et al., 2020; Seagren and Schoenbohm, 2021).

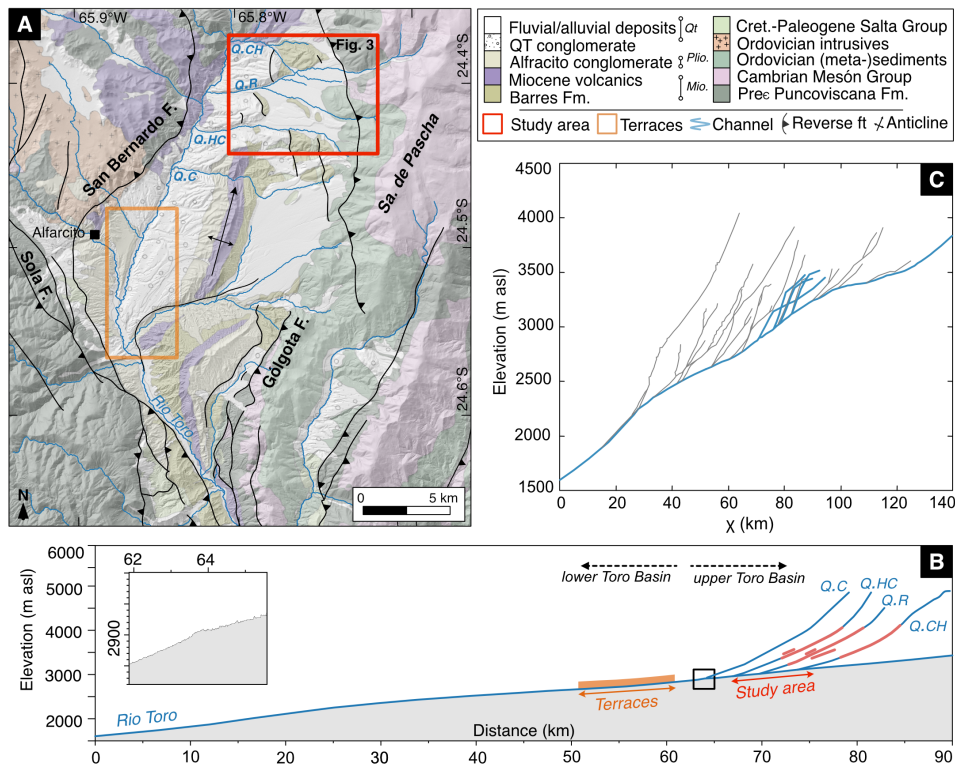
2.1 Geology and tectonic setting

The upper Toro Basin is confined by three reverse-fault bounded basement ranges: 1) the Cumbres de Zamaca bounded by the west-dipping Solá Fault in the west, 2) the Sierra de Almagro bounded by the northwest-dipping San Bernardo fault in the north, and 3) the Sierra de Pascha Ranges and the east-dipping Gólgota Fault in the east (Marrett and Strecker 2000) (Fig. 1, 2). The Solá fault has been active since at least the Pliocene, and tectonic deformation from the Miocene to mid-Pleistocene has been recorded along the San Bernardo and Gólgota faults (Marrett and Strecker 2000). The Gólgota fault reactivated after ca. 0.98 Ma (Hilley and Strecker 2005).

This study focuses on a suite of fans that emerge from the tributary catchments of the Sierra de Pascha and are located ~30 km upstream from the cut-and-fill terraces recording 100-kyr climate cyclicity described by Tofelde et al. (2017). The Pascha Ranges are characterised by meta-sediments of the Late Proterozoic-Cambrian Puncoviscana Formation and quartzites and shales of the Cambrian Mesón



141 Group (Schwab and Schafer 1976; García et al., 2013). Long term rock-uplift rates based on structural
142 reconstructions range between 0.4 and 0.6 mm/yr (Hilley and Strecker 2005).
143



144
145 **Figure 2.** Geology and topography of the upper Toro Basin. A) Geologic map with the alluvial fan sequence location (our
146 study area, Fig. 3) and cut-and-fill terraces described by Tofelde et al. (2017) outlined by red and orange rectangles
147 respectively. Other terraces extend discontinuously along the basin's channel length but remain undated. Map adapted from
148 Segemar 250k geological maps and Pingel et al. (2020). Abbreviations: Sa. – Sierra, F – Fault, Q.CH – Quebrada (mountain
149 stream) Chacra Huaico, Q.R – Quebrada Rosal, Q. HC – Quebrada Huasa Ciénaga, Q.C – Quebrada del Chorro, Q.Ca –
150 Quebrada Carachi. B) Long profile of Toro Basin with tributary profiles of upper basin study area. Upper and lower basin
151 reaches are indicated by dashed arrows. Full basin profile extracted from fluvial network outlined in Fig. 1. Alluvial fan and
152 terrace surfaces are projected onto profiles. Inset: Higher resolution plot of proposed knickzone at confluence between the Río
153 Toro and Quebrada del Chorro (outlined in main plot by black box). C) Chi-plot of all channels with a minimum drainage area
154 of 1 km² within the Toro basin using a reference concavity index of 0.45. Bold lines highlight the main river channel and
155 tributary catchments within our study area.
156

157 The Middle Miocene Barres Sandstone, interbedded with lava flows, and the Pliocene-Pleistocene
158 Alfarcito Conglomerates are exposed along a north-trending anticline, which lies between the fan
159 deposits and the Río Toro (Fig. 2A; Mazzuoli et al., 2008; DeCelles et al., 2011; Robledo et al., 2020).
160 Resistant Barres and Alfarcito units characterise several erosional surfaces that stand ~700 m above the
161 modern river channel. Incision into these tectonically deformed units by tributaries draining the Sierra
162 de Pascha is thought to have occurred after 0.98 Ma (Hilley and Strecker, 2005), the age of an
163 intercalated ash unit dated from the uppermost layers of the Alfarcito Conglomerate (Marrett et al.,



1994). Undeformed Quaternary conglomerates (also called ‘Terrace Conglomerates’) and fluvial/alluvial deposits either mantle or infill this tectonically deformed and eroded palaeotopography (Fig. 2; Marrett and Strecker, 2000; Hilley and Strecker, 2005). The Río Toro sets the local base level for the Pascha tributaries today (Tofelde et al., 2017).

2.2 Climatic setting

Moisture mainly governed by the South American Summer Monsoon (SASM) system is directed by the South American low-level jet (SALLJ) from the Atlantic Ocean and Amazon Basin to the Central Andes (Vera et al., 2006; Alonso et al., 2006; Bookhagen and Strecker 2008; Castino et al., 2017). The semi-arid Toro Basin is located towards the southern limit of this moisture conveyor and receives rainfall that ranges from ~900 mm/yr at the outlet to < 200 mm/yr in the basin headwaters (Fig. 1; Bookhagen and Strecker 2008). The Sierra de Pascha acts as an orographic barrier, causing the eastern flanks of the range to be comparatively wetter than the basin interior. The intensity of the SASM and resultant moisture supply to the Central Andes has been variable over time (see Baker and Fritz, 2015 for detailed review). Paleoenvironmental records from Argentina, Chile and Bolivia show that SASM precipitation has varied with changes in insolation over 19 to 25-kyr (precession) (Godfrey et al., 2003, Fritz et al., 2004, 2010; Placzek et al., 2006; Bobst et al., 2001) and 100-kyr (eccentricity) (Fritz et al., 2007; Gosling et al., 2008) cycles. The Central Andes are also subject to increased rainfall during periods of northern hemispheric cooling, whereby the Atlantic part of the intertropical convergence zone (ITCZ) is forced southward, bringing moisture with it (Broccoli et al., 2006; Mosblech et al., 2012; Novello et al., 2017; Crivellari et al., 2018). These cold and wet conditions correlate with phases of glacial advance and rising lake levels (Haselton et al., 2002; Vizzy and Cook, 2007; Martin et al., 2018; Mey et al., 2020).

Successions of glacial moraines are preserved within the Sierra de Pascha tributary catchments and are indicative of repeated late Quaternary glaciations (Tofelde et al., 2018). Glacial records proximal to the Toro Basin (24-27.2°S) underline the sensitivity of Andean glaciers to SASM precipitation intensity and temperature (Martini et al., 2017; Zech et al., 2017; Luna et al., 2018; D’Arcy et al., 2019a; Mey et al., 2020). The timing of regional glacial stages is invariably in phase with insolation cycles, periods of SASM strengthening and/or northern hemispheric events (e.g., Younger Dryas, Last Glacial Maximum) (D’Arcy et al., 2019a).

2.3 Basin sediment infilling and incision

Thick successions of sediment, together with subtle knickzones and hairpin turns in the Río Toro reflect a complex late Cenozoic history of basin filling and evacuation (Strecker et al., 2009; Hain et al., 2011; Vezzoli et al., 2012; Pingel et al., 2020), base level perturbations and tectonic deformation (Marrett and Strecker, 2000; Hilley and Strecker, 2005; Tofelde et al., 2017), and drainage reorganization (Seagren



200 and Schoenbohm, 2021; Seagren et al., 2022). Given our interest in the Quaternary deposits of the upper
201 Toro Basin, we focus our attention on how the basin has evolved over the last one million years.

202

203 After deposition of the Alfarcito conglomerates concluded at ca. 0.98 Ma, the Toro Basin was evacuated
204 to a base level lower than today (Hilley and Strecker, 2005). Renewed hydrological connectivity
205 between the Toro Basin and the Lerma Valley likely caused widespread basin sediment evacuation and
206 incision of the (paleo)topography. Uplift of the Sierra de Pascha Sur also recommenced sometime after
207 ca. 0.98 Ma (Hilley and Strecker, 2005). The newly uplifted range impeded the delivery of precipitation
208 to the basin interior, and by ca. 0.8 Ma, the semi-arid conditions of today were established (Kleinert and
209 Strecker 2001; Strecker et al. 2007; Pingel et al., 2020). The mechanically strong basement rocks, and
210 a potentially reduced sediment transport capacity, meant that incision was unable to keep pace with the
211 renewed rock uplift. This forced widespread aggradation and a decrease in relief upstream of the
212 Gólgota fault, and channel steepening within the bedrock gorge cutting through the Sierra de Pascha
213 Sur (Fig. 2; Hilley and Strecker, 2005; Strecker et al., 2009; García et al., 2013). External drainage
214 either became restricted or ceased at this time (Marrett et al. 1994; Hain et al., 2011; Pingel et al.,
215 2019a). Evidence for a similar sequence of events is seen in the Humahuaca, Casa Grande and
216 Calchaquí basins (23°S), where renewed range uplift reduced hydrological connectivity and caused
217 sediment infilling (Robinson et al., 2005; Hain et al., 2011; García et al., 2013; Pingel et al., 2013, 2016,
218 2019a; Streit et al., 2017; Seagren et al., 2022). Although there are some uncertainties about the exact
219 timing, connectivity between the Toro Basin and the foreland is thought to have been re-established due
220 to external base-level change (Seagren and Schoenbohm, 2021).

221

222 The Quaternary “Terrace Conglomerates” were deposited within the Toro Basin starting from ca. 0.94
223 Ma and are considered part of this phase of uplift-induced basin infilling (Hilley and Strecker, 2005). A
224 flight of six fluvial terrace levels in the lower basin are preserved between 20 and 200 m above the
225 modern Río Toro (Fig. 2). Cosmogenic exposure-age dating of terraces, burial dating of the sediments,
226 and zircon U-Pb ages of intercalated ashes from the terrace levels revealed multiple 100-kyr cut-and-
227 fill sedimentary cycles starting from ca. 500 ka (Tofelde et al., 2017). The phases of incision correspond
228 with cold, wet glacial periods, when sediment transport capacity apparently exceeded sediment flux,
229 whereas aggradation occurred when sediment transport was considerably reduced (Tofelde et al., 2017).
230 Moreover, the calculated net incision rate through the terrace sequence of 0.4 mm/yr from ca. 500 ka is
231 consistent with long term rock-uplift rates of the Sierra de Pascha Sur at the basin outlet (Hilley and
232 Strecker, 2005). Tofelde et al. (2017) thus concluded that while the renewed uplift of the Sierra de
233 Pascha Sur helped initiate the deposition of the Terrace Conglomerates, the periodicity of the cut-and-
234 fill cycles is best explained by orbitally driven climate forcing, with net incision likely associated with
235 the channel response to ongoing rock-uplift. Today, catchment-averaged erosion rates for catchments
236 draining the Sierra de Pascha range between <0.03 and 0.12 mm/yr (Tofelde et al., 2018).



237

238 **3. Methodology**

239

240 To evaluate past channel behaviour and landscape response to climate and/or tectonic forcing for the
241 upper Toro Basin, we applied **CRN** exposure dating to the suite of fan surfaces along the western front
242 of the Sierra de Pascha (Fig. 1, 2).

243

244 Alluvial fan CRN ages record the timing of active sediment deposition or surface stability between
245 periods of channel avulsion and incision (Dühnforth et al., 2007; D’Arcy et al., 2019b), which lead to
246 abandonment of the fan surface. This abandonment can occur due to changes in sediment supply
247 (Brooke et al., 2018; Tofelde et al., 2019), tectonic deformation and base level change (Ganev et al.,
248 2010; Mouslopoulou et al., 2017), climate-induced changes in water discharge (Steffen et al., 2010;
249 Savi et al., 2016) or drainage reorganization (Bufe et al., 2017). Because fan surfaces can remain active
250 for 10^{2-5} years before being incised (Cesta and Ward, 2016; Dühnforth et al., 2017; Ratnayaka et al.,
251 2019; Peri et al., 2022), the age distribution or minimum exposure age of boulders on an alluvial fan
252 surface will not necessarily tightly constrain the timing of abandonment. Instead, the distribution of
253 CRN ages, after excluding clear outliers, more likely reflects phases of fan activity, and at best, provide
254 a minimum age limit for the onset of incision leading to eventual surface abandonment (D’Arcy et al.,
255 2019b).

256

257 We mapped the upper Toro Basin fans using TanDEM-X (**12 m-resolution**) data and **Google Earth**
258 **imagery**. The stratigraphic relationships among the different fan surfaces were used to inform the
259 cosmogenic radionuclide (CRN) sampling strategy (e.g., McFadden et al., 1989; Hughes et al., 2010;
260 Hedrick et al., 2013).

261

262 Supporting topographic, fan and channel data were extracted from the **DEM** using TopoToolbox
263 functions in MATLAB (Schwanghart and Scherler, 2014) and geospatial toolboxes (**GRASS, GDAL**)
264 in **QGIS**. We also compiled a set of climate (Berger and Loutre, 1991; Baker et al., 2001; Imbrie et al.,
265 2006; Fritz et al., 2007; Wang et al., 2007; Lisiecki and Raymo, 2009), paleoenvironmental (Hilley and
266 Strecker, 2005; Tofelde et al., 2017; Pingel et al., 2020), glacial (Martini et al., 2017; Zech et al., 2017;
267 Luna et al., 2018; D’Arcy et al., 2019a; Mey et al., 2020) and geomorphic (Terrizzano et al., 2017;
268 Tofelde et al., 2017; Pingel et al., 2019b; Tobal et al., 2021; Peri et al., 2022; Milanez Fernandes, 2023)
269 records for the Andes to help contextualise our results.

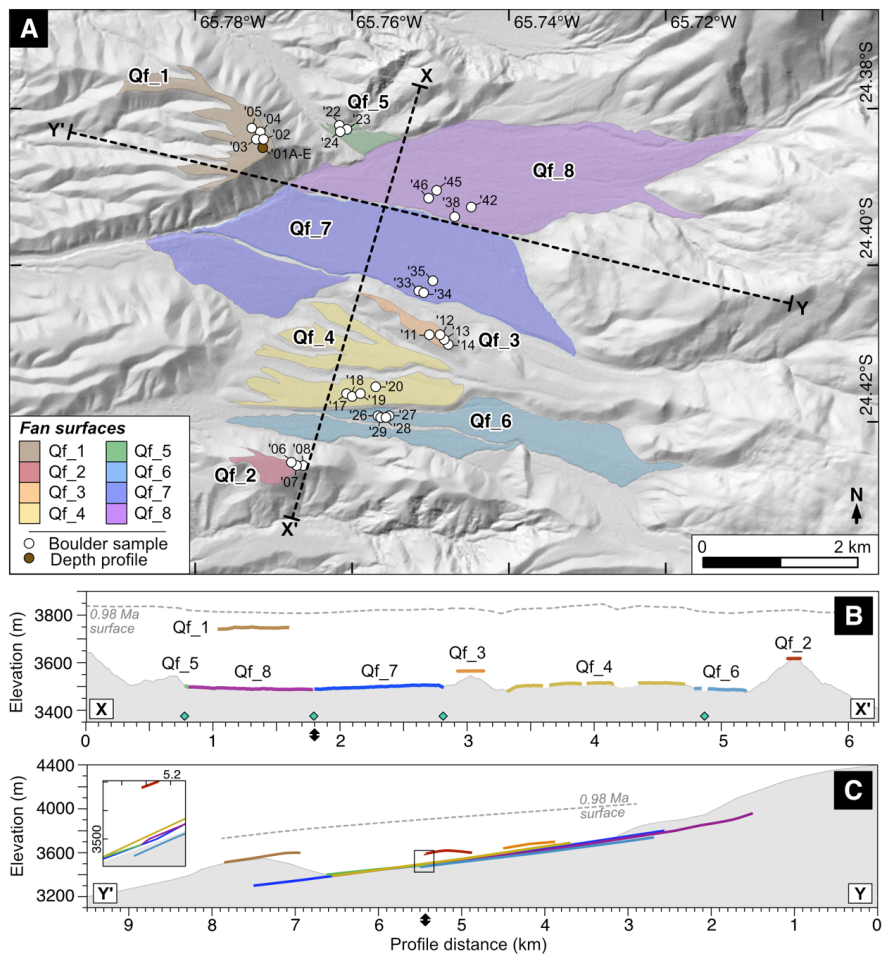
270

271 **3.1 CRN dating**

272 We collected a total of 30 quartzite boulder surface samples from eight fan surfaces (Fig. 3). Between
273 three and four boulders were sampled per surface. Each surface was named ‘Qf’ for ‘Quaternary fan’,



274 followed by a number which referred to its stratigraphic position. For example, Qf_1 sits ~200 m above
275 the modern river channel, and as the highest elevation surface of the study area, it was anticipated to be
276 the oldest fan.
277



278
279 **Figure 3.** Alluvial fan surfaces of the upper basin. A) Hillshade map of the dated fan surfaces with boulder and depth profile
280 sampling locations shown. Sample names have been abbreviated (e.g.: TB19_05: '05). X-X' and Y-Y' projection lines of Fig.
281 3B and 3C are represented by dashed black lines. B) Fan sequence stratigraphy shown by fan surfaces projected onto X-X'.
282 Qf_2 and Qf_3 surface widths are slightly exaggerated to improve visibility. Modern topography shaded in grey. The 0.98Ma
283 surface (grey dashed line) is modelled from sediment evacuation estimates of Hilley and Strecker (2005). Location of active
284 fluvial channels indicated by green diamond symbol. C) Fan surfaces projected onto Y-Y'. Inset plot provides higher resolution
285 view of projections (outlined by black rectangle). Projection line intersection is indicated by black double arrow.
286

287 Each sampled boulder was embedded within the fan surface, located away from channels, and within
288 the distal zone of the landform. This sampling strategy reduced the likelihood that the boulders were
289 sourced from adjacent hillslopes or were part of a depositional event following landform abandonment
290 (D'Arcy et al., 2019b; Orr et al., 2021). The sampled boulders were the largest, freshest boulders that



we were able to identify within the distal zone. However, we cannot definitively discount the possibility that the boulders experienced some weathering, surface spallation or fracturing in the past.

We removed between 400 and 1000 g of sample from the upper three centimetres of each boulder surface. The samples were crushed and then sieved to isolate the 250–500 μm grainsize fraction needed for CRN dating. Sample cleaning, purification, extraction and oxidation of ^{10}Be , and target preparation for AMS measurement was conducted in the Helmholtz Laboratory for the Geochemistry of the Earth Surface (HELGES) at the German Research Centre for Geosciences (GFZ-Potsdam) using the procedures outlined by von Blanckenburg, (2004) and Wittmann et al. (2016). AMS measurements were completed at the Cologne AMS facility at the University of Cologne, Germany.

Exposure ages derived from *in situ* produced ^{10}Be concentrations were calculated using the CREP online calculator (Martin et al., 2017) with the regional reference (SLHL) production rate of $3.74 (\pm 0.09)$ at/g yr for the high-elevation (> 3400 m asl) Central Andes (Blard et al., 2013; Kelly et al., 2015; Martin et al., 2015), and the LSD scaling scheme (Lifton et al., 2014). Further information about the boulder samples, the CRN laboratory procedure, blank ratios, and age calculation is provided in Supplement 1 and 2.

The probabilistic model for inferring the timing of fan surface abandonment from D'Arcy et al. (2019 b) was applied to fans with exposure ages of less than ca. 300 ka. The model uses the exposure ages of boulders on the fan surface to generate a probability distribution of abandonment ages and a most probable abandonment age. The model was not applied to older fan surfaces, which have large age distributions (>100 kyr range) and likely have some inheritance and/or surface erosion (Phillips et al., 1990; Tobal et al., 2021). Working with chronological data at this coarse resolution over 10^{5-6} -year timescales means that even the most sophisticated inheritance/erosion models are limited in their ability to estimate the timing of landform abandonment (e.g., Prush and Oskin, 2020; Dortch et al., 2022). For the Toro fans where this applies, we use the age distribution, stratigraphic order of the fans, and youngest exposure age as a guide for the timing of abandonment.

3.2 ^{10}Be depth profile

To help substantiate our new ^{10}Be boulder dataset we also resampled the Qf_1 ^{10}Be depth profile, referred to as P6b by Tofelde et al. (2017), and corresponding to their terrace level T6. The original profile was limited to five samples, which were sampled over relatively broad depth intervals (0–10cm, 18–28 cm, 25–81 cm, 82–164 cm, 164–210 cm). To obtain more highly resolved ^{10}Be data for this surface, particularly in the upper 100 cm, five samples of > 65 pebbles each were extracted from the following depth intervals (cm): 0–10, 20–30, 40–50, 60–70 and 115–125. The pebble samples were



crushed and sieved, and the 500–1000 μm fraction was reserved for CRN dating. Subsequent laboratory procedures followed that of the boulder samples.

The Qf_1 ^{10}Be depth profile, using combined ^{10}Be data from this study and from Tofelde et al., (2017), was used to determine an exposure age using the Hidy et al. (2010) Monte Carlo simulator. Further details are provided in Supplement 1 and 2.

4. Results

We use the upper Toro Basin alluvial fan elevations, surface characteristics, and CRN ages to identify two generations of fan surfaces. The studied fans are predominantly matrix-supported conglomerates with sub-angular to rounded pebble and cobble clasts. Weathered desert pavements cap many of the fan surfaces; a layer of finer sands and gravels are overlain by pebbles, cobbles, and boulders (e.g., McFadden et al., 1989; Tofelde et al., 2017).

The Generation 1 (G1) fan surfaces, comprising Qf_1 through 4, are stratigraphically the highest in the record and are positioned ~200 to 50 m above the modern river channel(s) (Fig. 3). The fan surfaces are moderately to highly weathered, with some evidence of surface boulder spallation (Fig. 4). With a few rare exceptions, the G1 sampled boulders are smaller than those sampled from the lower Generation 2 (G2) surfaces. The G1 and G2 boulders have b-axis lengths which range from 30 to 80 cm and 30 to 140 cm, respectively (Supplement 2). The CRN exposure ages from the G1 surfaces range between ca. 970 and 340 ka (Table 1; Fig. 5, 6).

G2 is comprised of fans Qf_5 through 8, which have surfaces within 10 m elevation of the modern channel(s) (Fig. 3). These moderately weathered surfaces retain debris flow deposits, evidence of past channel avulsion and sparse human infrastructure (e.g., stone walls). The CRN exposure ages of this younger fan generation range between ca. 100 and 20 ka, with estimated surface abandonment ages after ca. 70 ka (Table 1; Fig. 7).



Table 1. Sample properties, measured ¹⁰Be concentrations and calculated exposure ages of each sampled boulder from the Toro fans. Further sample and age calculation details are provided in the Supplement 2 and 3.

Sample	Location		Elevation (m asl)	Sample thickness (cm)	Shielding correction	Be-10 concentration		Be-10 exposure ages	
	Latitude (°S)	Longitude (°W)				Concentration (10 ⁶ at/g SiO ₂)	Uncertainty (10 ⁶ at/g SiO ₂)	Age (ka)	Uncertainty (ka)
Qf_1									
TB19_02	-24.38492	-65.76890	3556	1	0.990	24.20	0.78	966.63	109.78
TB19_03	-24.38492	-65.76890	3556	1	0.990	16.02	0.52	593.11	59.10
TB19_04	-24.38492	-65.76890	3556	1	0.990	22.33	0.72	884.41	95.34
TB19_05	-24.38492	-65.76890	3556	1	0.990	16.97	0.55	639.17	63.94
Qf_2									
TB19_06	-24.42522	-65.76775	3560	1	0.999	11.36	0.37	391.94	37.91
TB19_07	-24.42566	-65.76682	3570	2	0.999	17.00	0.55	631.77	64.10
TB19_08	-24.42568	-65.76607	3581	2	0.999	10.18	0.33	336.94	33.17
Qf_3									
TB19_11	-24.40882	-65.75023	3644	1	0.998	15.45	0.50	533.56	52.88
TB19_12	-24.40918	-65.74864	3658	3	0.998	18.06	0.59	651.82	66.21
TB19_13	-24.40976	-65.74810	3660	3	0.998	17.77	0.58	634.67	64.63
TB19_14	-24.41011	-65.74773	3673	3	0.998	11.18	0.37	361.38	35.49
Qf_4									
TB19_17	-24.41665	-65.76059	3509	1	0.999	14.73	0.48	548.44	54.60
TB19_18	-24.41675	-65.76000	3512	2	0.999	17.26	0.56	679.67	68.23
TB19_19	-24.41654	-65.75923	3519	3	0.999	19.06	0.61	778.81	79.15
TB19_20	-24.41533	-65.75681	3541	1	0.999	21.41	0.69	847.34	90.30
Qf_5									
TB19_22	-24.38245	-65.76145	3404	2	0.990	2.02	0.07	70.63	6.28
TB19_23	-24.38263	-65.76109	3407	2	0.995	2.34	0.08	82.69	7.35

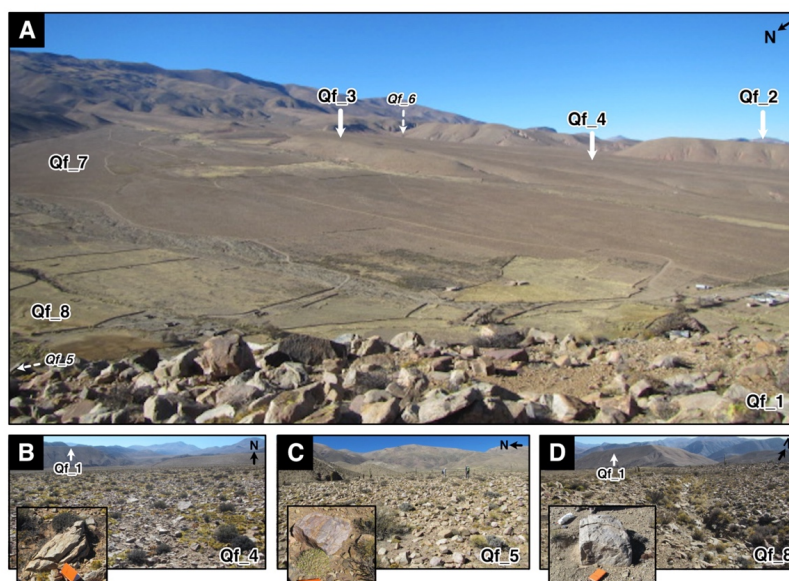


TB19_24	-24.38275	-65.76144	3405	3	0.995	2.77	0.09	98.81	8.82
Qf_6									
TB19_26	-24.41923	-65.75623	3531	2	0.998	2.16	0.07	69.97	6.27
TB19_27	-24.41921	-65.75578	3532	1	0.998	2.52	0.08	81.85	7.31
TB19_28	-24.41924	-65.75569	3541	2	0.998	2.22	0.08	71.11	6.46
TB19_29	-24.41941	-65.75652	3525	3	0.998	2.47	0.08	82.00	7.33
Qf_7									
TB19_33	-24.40346	-65.75108	3557	1	0.998	1.22	0.04	38.78	3.46
TB19_34	-24.40371	-65.75107	3555	2	0.998	1.87	0.06	59.28	5.36
TB19_35	-24.40203	-65.74977	3563	3	0.998	2.11	0.07	66.94	6.13
Qf_8									
TB19_38	-24.39402	-65.74711	3533	1	0.997	1.43	0.05	44.34	4.08
TB19_42	-24.39275	-65.74500	3553	1	0.997	1.43	0.05	43.65	4.04
TB19_45	-24.39043	-65.74940	3510	1	0.997	0.63	0.02	22.37	1.85
TB19_46	-24.39140	-65.75027	3502	1	0.997	1.44	0.05	45.32	4.212

1: LSD scaling scheme (Lifton et al., 2014), ERA40 Atmosphere Model (Uppala et al., 2005), LSD framework for geomagnetic correction (Lifton et al., 2014), Reference (SLHL) production rate: 3.74±0.09 at/g/yr. Sample density: 2.75 g cm⁻³. Erosion: 0 mm yr⁻¹



377



378

379 **Figure 4.** Images of the alluvial fan sequence of the upper Toro Basin. A) Image taken from Qf_1 surface (facing SE) with
 380 fan surfaces labelled. Italicized text with arrows indicates location of surfaces that are not clearly in shot. B) Qf_4 surface.
 381 Inset image of sampled boulder TB19_19. C) Qf_5 surface. Inset image of sampled boulder TB19_22. D) Qf_8 surface. Inset
 382 image of sampled boulder TB19_44. Images B–D encompass full age range of sampled surfaces. Further images of the fan
 383 surfaces and ^{10}Be samples are provided in Supplement 3.

384

385 4.1 Generation 1

386 Qf_1 is the highest fan surface of the record (~200 m above the modern channel), which extends from
 387 the Quebrada Rosal tributary catchment. The fan comprises part of the Quaternary conglomerates,
 388 which overlie the Barres Sandstone Formation (Fig. 2, 3). The depth profile is composed of four
 389 sedimentary units that coarsen with depth: silts and fine sands (0–20 cm), fine-coarse sand (20–60 cm),
 390 coarse sand and gravel (60–180 cm) and gravels (>180 cm). Consistent with the original profile, the
 391 new ^{10}Be sample concentrations decrease exponentially with depth (Fig. 5; Table 2). Qf_1 has a
 392 Bayesian most-probable exposure age of 715.8^{+35}_{-217} ka (2 σ upper age: 750.8 ka, 2 σ lower age: 498.8
 393 ka) and $0.26 \pm 0.42 \times 10^6$ atoms/g of inheritance. Within the simulator, we constrained fan surface erosion
 394 and inflation by setting the erosion rate to range between -0.02 and 0.2 cm/ka and using maximum and
 395 minimum erosion thresholds of -10 and 50 cm, respectively. While this modelled exposure age is
 396 consistent with the age estimated earlier by Tofelde et al. (2017) of 732^{+53}_{-56} ka assuming a stable
 397 surface, or 644^{+43}_{-49} ka accounting for surface inflation, Tofelde et al. (2017) preferred the exposure
 398 age they derived from surface pebbles of 453 ± 33 ka.

399

400 The exposure ages of boulder samples TB19_03 and TB19_05 are in agreement with the depth profile
 401 results, yielding exposure ages of 639.17 ± 63.94 and 593.11 ± 59.10 ka (2 σ uncertainty). The two



remaining boulders (TB19_02, TB19_04) yielded older exposure ages of 966.63 ± 109.78 and 884.41 ± 95.34 ka.

404

Table 2. Sample depths and measured ^{10}Be concentrations of Qf_1 depth profile. Fan age calculated with the Hidy et al. (2010) Monte Carlo depth profile simulator was 715.8^{+35}_{-217} ka. Inheritance measured: $0.26 \pm 0.42 \times 10^6$ at/g.

407

Sample ¹	Sample depth		Be-10 concentration	
	Depth (cm)	Uncertainty (cm)	Concentration (10^6 at/g SiO_2)	Uncertainty (10^6 at/g SiO_2)
BBC-0	5	5	14.70	0.18
TB19_01A	5	5	14.97	0.48
BBC-1	23	5	11.80	0.11
TB19_01B	25	5	12.14	0.39
TB19_01C	45	5	10.88	0.35
BBC-2	53	28	7.76	0.07
TB19_01D	65	5	8.76	0.28
TB19_01E	120	5	4.94	0.16
BBC-3	123	41	5.21	0.06
BBC-4	187	23	2.30	0.03

1: TB19_01A-E from this study. 'BBC-1-4' from Tofelde et al. (2017).

408

Surface Qf_2, the second highest surface (ca. 130 m above the closest modern channel), also overlies the Barres Sandstone and likely extends from the Quebrada Huasa Ciénaga and Quebrada del Chorro catchments. CRN exposure ages from three boulders range from 631.88 ± 64.10 to 336.94 ± 33.17 ka.

413

The Qf_3 surface is positioned ca. 60 m above the closest modern channel and extends from the Quebrada Rosal tributary catchment. The surface yields three CRN boulder exposure ages that cluster between 651.82 ± 66.21 and 533.56 ± 52.88 ka, and one younger age of 361.38 ± 35.49 ka.

417

Qf_4 has a highly dissected fan surface which is the lowest stratigraphically of the G1 fans; the fan is positioned ca. 40 m below the Qf_3 surface and ca. 30 m elevation above the modern channel. Four boulder exposure ages range from 911.61 ± 100.27 to 548.44 ± 54.60 ka.

421

4.2 Generation 2

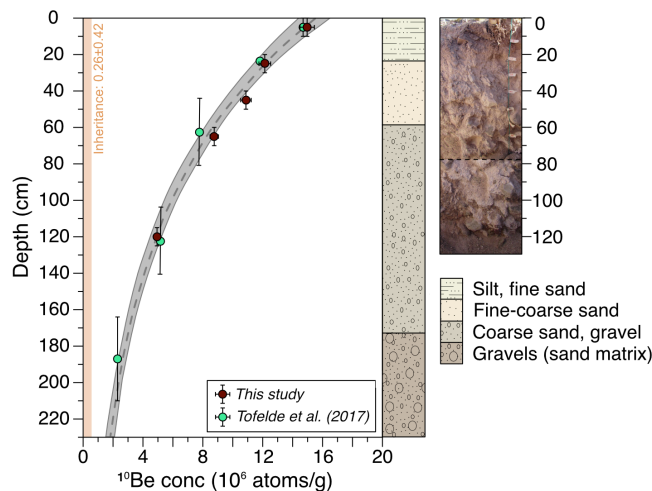
Qf_5 is a small G2 surface that sits ca. 10 m above the neighboring Qf_8 fan. Qf_5 has three exposure ages that range from 98.81 ± 8.82 to 70.63 ± 6.28 ka, with a most probable abandonment age of $61.8^{+13.5}_{-33.6}$ ka (no ages excluded as outliers).

426

Qf_6's surface is characterized by moderately weathered debris flow deposits with clusters and elongated ridges of boulders. Exposure ages range between 82.00 ± 7.33 and 69.97 ± 6.27 ka from the



429 four boulders, with an estimated surface abandonment age of $66.2^{+11.0}_{-17.5}$ ka (no ages excluded as
430 outliers).



431
432 **Figure 5.** ^{10}Be concentration with depth for Qf_1 profile alongside sedimentary log and stitched field image of the profile pit.
433 Each sample was collected over a depth range represented by a vertical error bar. Horizontal error bar represents the 1σ
434 analytical uncertainty for the nuclide concentration. The Hidy et al. (2010) Monte Carlo simulator fit 100,000 curves (grey
435 shading) to profile and generated most probable fit (grey dashed line). Modelled inheritance is shown by orange line. *Profile
436 6b data, rather than 6a, from the supplementary materials is used in simulation, due to the mislabelling of the profile in Fig. 4
437 of Tofelde et al. (2017).
438

439 Despite Qf_7 being located within 5 m elevation of the youngest G2 fan Qf_8, this large fan appears
440 more weathered than Qf_8. Qf_7 has CRN exposure ages of 66.94 ± 6.13 , 59.28 ± 5.35 and $38.78 \pm$
441 3.47 ka. The surface abandonment ages including and excluding the youngest age are $33.9^{+7.4}_{-25.1}$ and
442 $52.9^{+11.0}_{-16.3}$ ka, respectively.

443
444 Surface Qf_8 yielded a cluster of older ages that range between 45.32 ± 4.2 and 43.65 ± 4.04 ka and a
445 single younger age of 22.37 ± 1.83 ka. Abandonment ages including and excluding the youngest age
446 are $19.4^{+4.1}_{-19.4}$ and $42.4^{+6.5}_{-7.5}$ ka, respectively. The surface is covered with relatively unweathered
447 debris flow deposits and large varnish-free boulders.

448 5. Discussion

449
450 While there are some nuances to the Toro Basin fan record, our new CRN dataset enables us to identify
451 significant phases of net incision since ca. 0.98 Ma, capture the channel response to external forcing
452 over a range of timescales and cyclicities, and gain further insight into the late Quaternary evolution of
453 the Toro Basin.
454

455



5.1 Timing of alluvial fan development and abandonment

CRN age uncertainties on the order of 10^{4-5} years and a wide range of fan exposure age distributions on individual surfaces present some challenges when interpreting the Toro fan chronostratigraphy, which is crucial for comparison with potential external forcing conditions. Constraining the geological uncertainties of the CRN ages, particularly for old fan surfaces, is often challenging (Owen et al., 2014). For this reason, we use geological, topographic and paleoenvironmental data alongside the ^{10}Be data to interpret the alluvial fan record. The coarse resolution of the G1 ^{10}Be record means that while we can reflect upon long term shifts in channel behaviour for the upper Toro Basin, we must exercise caution when linking this record to specific forcing or events (Gray et al., 2014; Dünnforth et al., 2017; Orr et al., 2021). Pairing the ^{10}Be record with cosmogenic ^{21}Ne in the future may help to decipher some of the complexities in the exposure histories of the boulders; ^{21}Ne is well suited for quantifying long term landscape change in arid, low erosion environments (Dunai et al., 2005; Ma and Stuart, 2018).

5.1.1 Fan Generation 1

The ~200-m elevation difference between the highest and lowest fan surface among Generation 1 means that the G1 surfaces could not have been active simultaneously (Fig. 6). Substantial inheritance and/or erosion has therefore likely affected individual boulders from these surfaces and offers one explanation for the broad spread in ages (>400 kyr) for each.

Pairing the Qf_1 ^{10}Be depth profile with the surface boulder exposure ages means that we can more robustly constrain the oldest phase of fan development within the study area and use it as a benchmark when evaluating the remainder of the G1 fan record. The most recent phase of Qf_1 surface activity and/or stability is constrained by the depth profile data and two boulders to between ca. 750 and 600 ka. In this case, we believe that CRN inheritance may explain why the remaining two boulders (TB19_02, TB19_04) from this surface yield exposure ages that exceed ca. 800 ka. Considering the whole suite of boulder ages for the G1 fans, which mostly exceed 500 ka, we find it unlikely that the age of 453 ± 33 ka (based on surface pebbles) originally reported by Tofelde et al. (2017) for Qf_1 is correct.

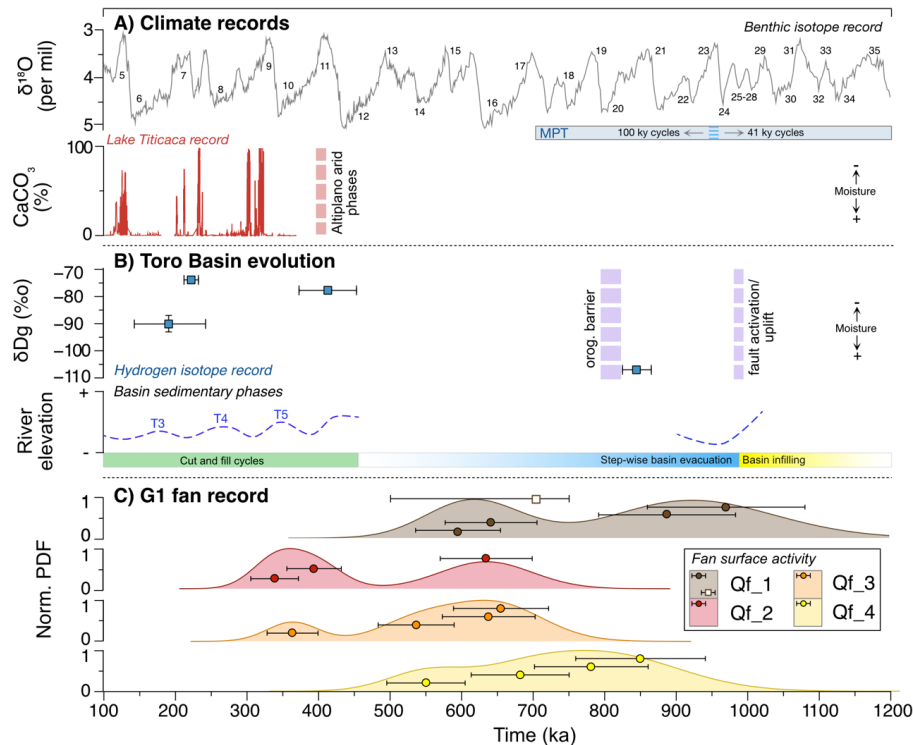


Figure 6. Comparison between the G1 fan ^{10}Be dataset and records of Toro Basin evolution and climate. A) Benthic isotope record (Lisiecki and Raymo 2009) displayed alongside Marine Isotope Stages (MIS) and Mid-Pleistocene Transition labelling and the Lake Titicaca sediment core record (CaCO_3 concentration) from Fritz et al. (2007). B) Toro basin evolution. Climatic variability represented by hydrogen isotope record of Pingel et al. (2020). Basin sedimentary and tectonic phases plotted with respect to inferred river elevation over time, as observed by this study and described by Hilley and Strecker (2005), Tofelde et al. (2017) and Pingel et al. (2020). Fluvial terrace record (T3-6) from Tofelde et al. (2017). C) ^{10}Be surface boulder ages and normalised probability density functions of the G1 surfaces. Horizontal error bars represent the 1σ uncertainty for the exposure ages. Bayesian modelled surface age of Qf_1 (715.8 $^{+35}_{-217}$ ka) derived from depth profile (Fig. 5) is denoted by square point.

Given the stratigraphic positions of Qf_2 and Qf_3, we think that it is unlikely that active streams were present on these surfaces after ca. 400 ka. For this reason, we suggest that the younger ages for these surfaces are the result of erosion. These surfaces also must be older than surface Qf_4, which yielded a youngest age of ca. 550 ka.

Inheritance also likely explains the old (>750 ka) boulders on Qf_4, which is stratigraphically younger than Qf_1 and cannot have been active at the same time.

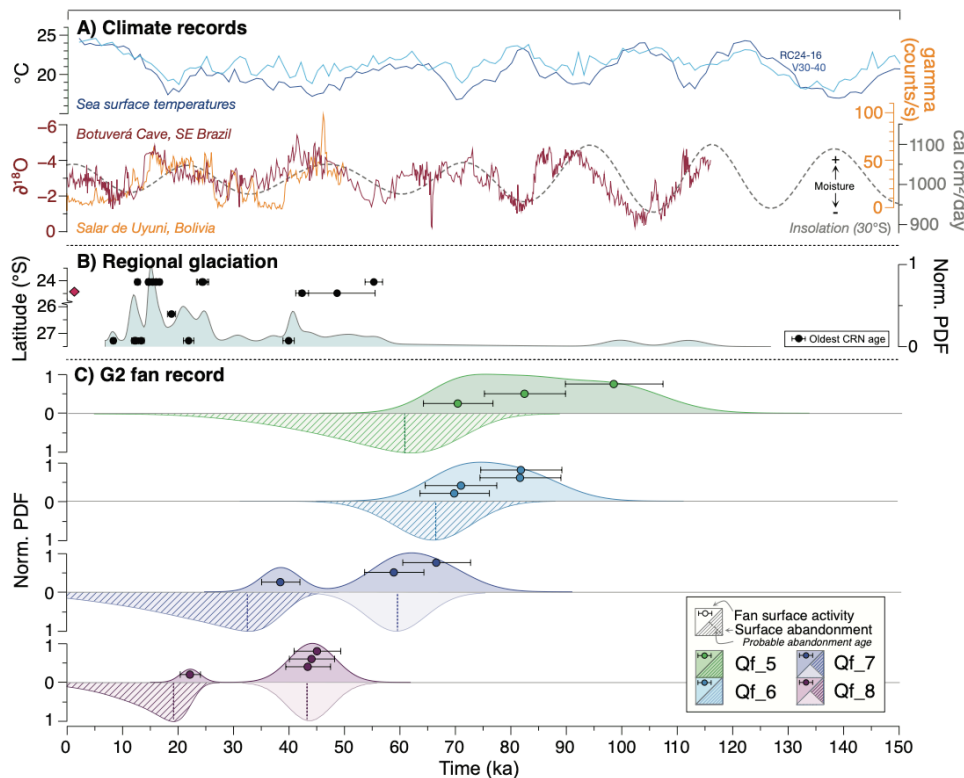


Figure 7. Comparison between the G2 fan ^{10}Be dataset and regional climate and glacial records. A) Climate records. Sea surface temperatures from Imbrie et al. (2006), insolation from Berger and Loutre (1991), Botuverá Cave, SE Brazil speleothem record from Wang et al. (2007) and Salar de Uyuni, Bolivia lake record from Baker et al. (2001). B) CRN glacial chronologies from the Central Andes: Nevado de Chañi (24°S, 65.7°W, Martini et al., 2017, Mey et al., 2020), Quevar Volcano (24.4°S, 66.8°W, Luna et al., 2018), Sierra de Quilmes (26.2°S, 66.2°W, Zech et al., 2017) and the Sierra Aconquija (27.2°S, 66.1°W, D'Arcy et al., 2019a). Location of Toro Basin (24.4°S, 66.7°W) is indicated by red diamond symbol. C) ^{10}Be boulder ages and normalised probability density functions of the G2 surfaces. Horizontal error bars represent the 1σ uncertainty for the exposure ages. Normalised PDF of fan surface abandonment (hashed shading) calculated using the D'Arcy et al. (2019b) probabilistic model for fan surface abandonment. Surface abandonment for Qf_7 and Qf_8 without youngest boulder ages (TB19_33 and TB19_45, respectively) shown by PDFs with opaque solid shading. Most probable abandonment ages denoted with dashed vertical lines: Qf_5: 61.8 $^{+13.5}_{-33.6}$ ka, Qf_6: 66.2 $^{+11.0}_{-17.5}$ ka, Qf_7: ca. 33.9 $^{+7.4}_{-25.1}$ ka (52.9 $^{+11.0}_{-16.3}$ ka), Qf_8: 19.4 $^{+4.1}_{-19.4}$ ka (42.4 $^{+6.5}_{-7.5}$ ka).

Given these complexities in the fan chronostratigraphy, rather than identifying discrete phases of aggradation and incision for each fan surface, we suggest that the G1 fan record can instead be used to capture an extended phase of net incision within the Sierra de Pascha tributaries. By comparing the G1 fan record with the modelled palaeotopography of Hilley and Strecker (2005), we estimate that ~100 m of net incision (~0.01 mm/yr) occurred within the upper basin between ca. 0.98 Ma and 800 ka, at which point the Qf_1 surface became active (Fig. 3B, C, Fig. 8). Approximately 200 m of net incision (~0.07 mm/yr) then followed between ca. 800 ka and the complete abandonment of the G1 fans by ca. 500 ka (when adjusting for age outliers) (Fig. 6), which signals the significant stepwise evacuation of sediment from the upper Toro Basin at this time.



5.1.2 Fan Generation 2

The G2 record reveals that after a hiatus in the geomorphic record ca. 500 and 100 ka, fan aggradation and incision is recorded throughout several of the Sierra de Pascha tributaries (Fig. 8). Rather than recording continuous fan activity since ca. 110ka, the distribution of ages for G2 instead likely captures multiple distinct phases of deposition. The G2 fan surfaces have much tighter constrained age distributions (ca. 21 to 40 kyr) compared to the G1 fans, with two G2 fans showing what may be young outliers; the boulders are therefore less likely to be affected by inheritance, but the young outliers may be affected by erosion or tilting by human or animal activity.

5.2 Drivers of alluvial channel system change and fan/terrace formation

Before we can explore some of the possible explanations for the alluvial system change recorded in the Toro Basin, we must first consider the specific local conditions needed to help explain the G1 (ca. 800 to 500 ka) and G2 (ca. 100 to 20 ka) fan generations in the upper basin, as well as the fluvial terrace sequence (ca. 370 ka to <75 ka) in the lower basin. Changes in water or sediment discharge, governed by climate, can affect channel slopes and prompt adjustments to the channel bed elevations through incision or aggradation (Howard, 1982; Wickert and Schildgen, 2019; Tofelde et al., 2019). Nevertheless, net incision is essential to preserving the geomorphic record of aggradation-incision cycles. Otherwise, subsequent aggradational phases are likely to bury earlier landforms. Net incision can occur through the channel response to ongoing rock uplift or base level fall (Simpson and Castelltort, 2012), the latter of which may include renewed incision through an aggraded sequence of sediment downstream. While autogenic processes, such as channel avulsion and meander cut-offs may also play a role in channel incision and the formation of discrete fan lobes or terraces (Nicholas and Quine, 2007; Ventra and Nichols, 2014), we consider the scale of channel incision associated with the features of interest (ranging from ca. 10 to hundreds of meters) is beyond the scope of purely autogenic behavior. Below, we consider how climate-modulated changes to water and sediment discharge, together with events that can drive net incision, may have helped to generate, and preserve multiple generations of fans and terraces within the Toro Basin.

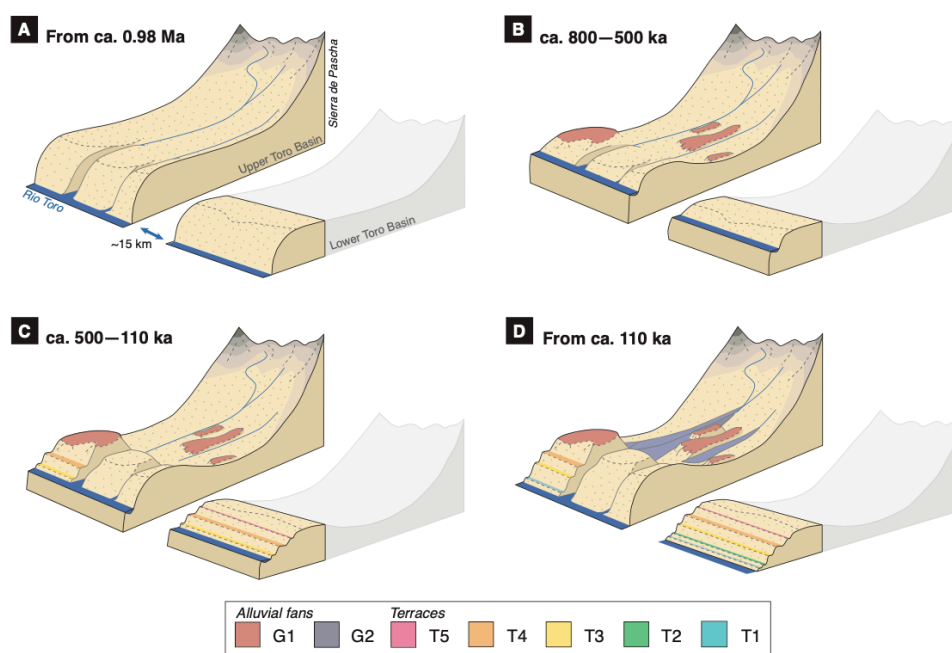
5.2.1 Fan formation from ca. 800 to 500 ka

The development, entrenchment, and eventual abandonment of the G1 fans could be part of the landscape response to enhanced rock-uplift of the Sierra de Pascha Sur, starting no later than ca. 800 ka (Fig. 8) (Clarke et al., 2010; Mather et al., 2017; Mouchéné et al., 2017). However, another mechanism is likely at play because the averages rates of incision between ca. 800 and 500 ka (0.8 mm/yr) as recorded by the G1 fans, exceed the estimated rock uplift rates of 0.4 – 0.6 mm/yr (Hilley and Strecker, 2005), and tectonic uplift alone is unlikely to be pulsed in a manner that would generate multiple fans. More likely, both climate forcing and tectonic forcing combine to produce and preserve the G1 fan sequence. Over the same period, curiously, no terraces are detected in the lower Toro Basin. Three



possible explanations for this absence (which are not mutually exclusive) include: (1) due to their more central position within the basin, the lower reaches of the Río Toro were not strongly affected by rock uplift, meaning that any changes in river-channel elevation are not persevered in the geomorphic record due to low or a lack of net incision; (2) channels in the lower Toro Basin continued to experience aggradation or remained stable at this time, due to feedbacks in the system whereby incision upstream caused a pulse of sediment for downstream reaches; or (3) the response time of the Río Toro within the lower basin was substantially longer than the forcing period of the aggradation-incision cycles, meaning perturbations to the channel-bed elevation due to climate forcing would not have reached so far downstream.

571



572

Fig. 8. Cartoon illustrating periods of aggradation and incision in the upper and lower Toro Basin from ca. 0.98 Ma. Area of Lower Toro Basin block shaded in grey was not part of this study. A) From 0.98Ma: Base level lowered to present day levels, following the deposition of Alfarcito Conglomerates. Renewed hydrological connectivity likely led to extensive sediment evacuation and incision of (paleo)topography. Deposition of Quaternary Terrace Conglomerates started from 0.94 Ma (Hilley and Strecker, 2005). B) ca. 800–500 ka: G1 fan formation and abandonment during a phase of net incision in the upper basin, linked to the MPT. No significant geomorphic change recognised in the lower basin. C) ca. 500–110 ka: 100-kyr cycles of aggradation and incision recorded by lower basin cut-and-fill terraces (T5, T4, T3). No significant geomorphic change recognised in the tributaries of the upper basin. D) From ca. 110 ka: G2 fan formation and abandonment in the upper basin, linked to ca. 21/40 kyr climate cycles. Continuation of 100-kyr cycles recorded by lower basin terraces (T2, T1).

582

To elaborate on the first possibility, the Sierra de Pascha catchments are positioned behind and perpendicular to the axis of an elevated northward-plunging anticline (Fig. 2A). In concert with the work by Hilley and Strecker (2005), we suggest that channel incision through the resistant anticline accelerated sometime between 0.98 and 0.8 Ma. Once this incision propagated upstream and to the east



587 of the anticline, the removal of weakly consolidated sedimentary units in the upper basin was likely
588 efficient (Hilley and Strecker, 2005). The evolving topography of the anticline could therefore help to
589 explain the net incision needed in the upper Toro Basin to preserve the alluvial fan surfaces between ca.
590 800 to 500 ka, and why terrace levels in the lower basin are not recognised during this time interval.

591

592 To elaborate on the second and third possibilities, as late Quaternary glaciations were limited to the
593 Pascha tributary headwaters (< 5 km from headwall), the hillslope geomorphic response to prolonged
594 and intensified glaciation may have been very localized (Tofelde et al., 2018). This is apparently true
595 for the Iglesia and Calingasta Basins in the Western Precordillera where the tributaries, rather than the
596 main basin record incision following the Mid-Pleistocene Transition (Terrizzano et al., 2017; Peri et al.,
597 2022). Following this argument, the response time of the Río Toro's long profile to the 100-kyr climate
598 cycles after the Mid-Pleistocene Transition (ca. 1.2 to 0.8 Ma) may have been substantially longer than
599 the period of external forcing. If true, this implies that while upstream reaches of the channel may have
600 experienced no (or a very low amplitude) aggradation/incision cycles (Allen, 2008; McNab et al., 2023).
601 Alternatively, feedbacks within the system could lead to differences not only in the magnitude of
602 aggradation/incision, but also the timing. For example, in southwest Peru, Steffan et al. (2009, 2010),
603 interpreted aggradation in downstream reaches of river channels during past wet climate periods to
604 result from pulses of sediment mobilized from hillslopes and upstream channel incision.

605

606 *5.2.2 Terrace formation from ca. 500 to 110 ka*

607 From ca. 500 to 110 ka in the upper Toro Basin, we find no record of fan formation (Fig. 8). Curiously
608 again, though, the lower Toro Basin exhibits a spectacular sequence of terraces showing 100-kyr
609 cyclicity starting from ca. 500 ka (Tofelde et al., 2017). If long channel response times explain the lack
610 of terraces from ca. 800 – 500 ka in the lower Toro Basin, to explain the terraces identified in the lower
611 basin ca. 500 ka (Tofelde et al., 2017), the channel response time must have changed. This could have
612 occurred as a result of incision in the upper Toro Basin, which would have narrowed the upstream river
613 valleys, consequently decreasing river response times and enabling aggradation-incision cycles to affect
614 channel reaches farther downstream (e.g., McNab et al., 2023).

615

616 While a shortened channel response time can explain the formation of terraces in the lower Toro Basin,
617 it does not explain the absence of terraces/fans in the upper basin over the same period. Consequently,
618 we next consider other factors that might lead to differences in fan/terrace preservation between the
619 upper and lower Toro basins.

620

621 Perturbations at the Río Toro outlet, such as a shift in base level, will propagate upstream over time,
622 thus driving the net incision needed to preserve variations in channel bed elevation in the terrace and
623 fan sequences. Alternatively, activity along the Gólgota Fault at this time may have adjusted the base



624 level for the trunk stream. Regardless of the exact trigger for base-level fall (e.g., renewed fluvial
625 connectivity, possibly enhanced by a drop in Lerma Valley lake level) (Malamud et al., 1996; González
626 Bonorino and Abascal, 2012), a net incisional wave would have propagated upstream from the lower
627 basin or outlet. That incision would have facilitated terrace preservation in the lower Toro Basin before
628 the incisional wave propagated upstream to the upper Toro Basin. Steepened reaches of both the trunk
629 stream and tributaries up to an elevation of ca. 3400 m (Fig. 2C) are consistent with an upstream
630 propagating wave of incision, which probably only recently reached the ca. 3300-m elevation of the G2
631 fan toes.

632

633 Consistent with this interpretation, both the upper and lower Toro basins preserve geomorphic evidence
634 of channel-bed elevation lowering after ca. 100 ka (terraces T2 and T1 in the lower Toro Basin; G2 fan
635 generation in the upper Toro Basin). Whereas T2 and T1 lie 40 m and 20 m respectively above the
636 modern Río Toro, the G2 fans are at most 10 m above their closest channel. This finding further supports
637 the idea that net incision is ongoing in the lower Toro Basin, probably keeping pace with the ongoing
638 uplift of the Sierra de Pascha Sur (Tofelde et al., 2017), but net incision has possibly only resumed
639 within the last ca. 110 to 50 kyr in the upper Toro Basin.

640

641 Other factors may have also played a role in the misaligned timing of fan/terrace formation in the upper
642 and lower Toro basins. Restricted hydrological connectivity or disconnectivity can lead to internal
643 variability in the nature and timing of a basin's geomorphic or sedimentary response to external
644 perturbations (Fryirs et al., 2007; Buter et al., 2022). For example, basin connectivity and geometry
645 appear to have disrupted the timing of climate-driven sediment transfer within the Humahuaca Basin of
646 NW Argentina during the last glacial cycles, leading to anti-phased timing of aggradation-incision
647 cycles along tributaries on either side of the valley (Schildgen et al., 2016). No fault lines, which can
648 influence connectivity (Guarnieri and Pirrotta, 2008; Brocard et al., 2012), intersect the channel network
649 between the alluvial fans and terrace levels of the Toro Basin (Fig 2) (Pingel et al., 2020). Nevertheless,
650 minor adjustments to the long profile of an alluvial channel network can be sufficient to affect the
651 internal connectivity of a basin (Savi et al., 2020). One such adjustment may include the tributary
652 junction fan at the Quebrada de Chorro outlet, which has created a diffuse knickzone in the Río Toro
653 long profile (Fig. 2B). As the fan has aggraded, it has pushed the main channel to the opposite valley
654 side, evidenced by a marked channel bend. The fan may therefore inhibit the coupling between the
655 upstream and downstream reaches of the trunk stream by disrupting the flow of sediment and (possibly)
656 water from the Sierra de Pascha tributaries and along the Río Toro (e.g., Harvey 2012). However, the
657 capacity of the fan to disrupt environmental signals moving through the basin may depend on the
658 direction of signal travel. For example, channel incision due to a climate-induced increase in water
659 discharge may continue to propagate downstream, regardless of a new sedimentary input from a major
660 tributary, unless the tributary fully dams the upstream section. However, if a wave of incision is instead



661 migrating upstream, a tributary junction fan may slow or disrupt its propagation (Savi et al., 2020).
662 Nevertheless, while sedimentary inputs from individual tributaries can affect the modern channel
663 profile, and may slow upstream-propagating incisional cycles, it is not clear whether such localized
664 features will play an important role in channel network evolution over longer (e.g., > 100 kyr)
665 timescales.

667 5.2.3 Fan formation since ca. 110 ka

668 All G2 surfaces were either stable or actively receiving sediment for some time during both cool, wet
669 glacial periods and warm, dry interglacials. Similar to the terraces in the lower basin (Tofelde et al.,
670 2017), the timing of G2 surface abandonment is restricted to glacial phases; enhanced moisture
671 availability due to an intensified SASM is likely to have amplified sediment transport and channel
672 incision (Baker and Fritz, 2015). Around the latitude of the Toro Basin, glacial moraine records in the
673 Central Andes show strong evidence for glacial advances at ca. 16 and 22–24 ka, with some evidence
674 also for advances at ca. 42 and 55 ka (D’Arcy et al., 2019a; Fig 7B). The stratigraphically highest
675 surfaces in G2, Qf_5 and Qf_6, show abandonment ages that are consistent with the timing of the oldest
676 glacial advances recorded in the moraine record (ca. 55 ka).

677
678 For surfaces Qf_7 and Qf_8, the timing of abandonment is harder to interpret, due to the difficulty in
679 knowing whether the youngest boulders on each surface are outliers due to erosion/rotation, or if they
680 represent a time of active deposition on the surface. Given the similarities in surface weathering between
681 Qf_6 and Qf_7, it is possible that Qf_7 was active at the same time as Qf_6 and Qf_5, and hence was
682 abandoned at a similar time (implying that the youngest boulder of Qf_7 is an outlier). If the young
683 boulder instead represents a real depositional age, then the abandonment of Qf_7 could be linked to the
684 ca. 22–24 ka glacial advance, coinciding with the northern hemisphere Last Glacial Maximum. The
685 abandonment of Qf_8 is similarly challenging to interpret, with abandonment potentially linked to either
686 the ca. 24 ka glacial advance (associated with the ‘Minchin’ wet climate phase of the Central Andes) if
687 the youngest boulder is excluded, or the ca. 16 ka glacial advance associated with Heinrich Stadial 1 if
688 not excluded.

689
690 While we reason that the two youngest ages from Qf_7 and Qf_8 are not outliers and instead reflect
691 later deposition events (see 5.1.2), we have also estimated the timing of surface abandonment without
692 them (Fig. 7). In this alternative record, the abandonment of three of the four fans fall between ca. 65
693 and 60 ka. This points to a modest phase of net incision in several Sierra de Pascha catchments during
694 a wet glacial period (Fritz et al., 2007).

695



Overall, the exposure age distributions and estimated abandonment ages appear to capture cycles of fan aggradation-incision with a periodicity of ca. 20 to 40 kyr. Considering the above tentative links between abandonment times and glacial advances, and that no known tectonic forcing in the Toro Basin can explain this cyclicity, the alluvial channel network is likely responding to precession (21-kyr) or obliquity-driven (40-kyr) climate cycles. Precessional forcing has been recorded within the sedimentary archives elsewhere in the Central Andes, including fluvial terraces in the Humahuaca Basin (23°S) (Schildgen et al., 2016) and alluvial fans in the Santa María Basin (26.5°S) (D'Arcy et al., 2018) in NW Argentina.

5.3 Impacts of the Mid-Pleistocene Transition on the Toro Basin

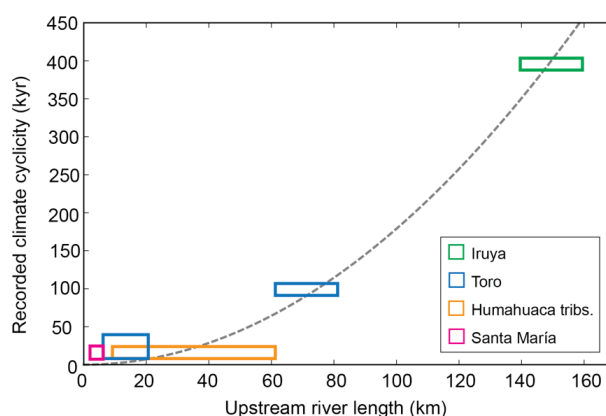
The G1 fan surfaces have CRN exposure ages that span several glacial-interglacial cycles (Fig. 6). Although our interpreted ages are too imprecise to associate with specific glacial phases, 100-kyr glacial moderation of aggradation-incision cycles is thought to have controlled fluvial terrace formation in the lower Toro Basin (e.g., Tofelde et al., 2017). In semi-arid landscapes and transport-limited systems, this finding is not unexpected, as geomorphic activity is invariably amplified during wetter, glacial periods (Harvey et al., 1999; Spelz et al., 2008; Cesta and Ward, 2016). Given the number of G1 fans ($n=4$) capturing the prolonged net incisional phase (>300 kyr), it is possible that eccentricity-driven cycles of aggradation and incision are also recorded in the upper Toro Basin.

Our net incisional phase between ca. 800 and 500 ka coincides with the onset of prolonged and enhanced global glacial cycles following the Mid-Pleistocene Transition (MPT, 1.2–0.8 Ma) which marked a shift in climate periodicity from 41 to 100 kyr cycles (Berger et al., 1999). The southward migration of the ITCZ at this time led to heightened moisture availability throughout the Central Andes (Haselton et al., 2002; Broccoli et al., 2006; Vizy and Cook, 2007). Alluvial channels in semi-arid regions of the Central Andes are found to respond quickly to marked shifts in precipitation such as this (e.g., Schildgen et al., 2016; Tofelde et al., 2017), which also appear to drive phases of enhanced sediment evacuation to the foreland (Fisher et al., 2023).

Enhanced incision linked to the MPT has also been recognised at other locations in the Central Andes (Fig. 1A), including the Casa Grande Basin (23°S) in the Eastern Cordillera, the Salinas Grandes Basin (23.5°S) of the Puna Plateau (Pingel et al., 2019b), and the Iglesia (30.5°S) and Calingasta (32°S) basins in the Western Precordillera (Terrizzano et al., 2017; Peri et al., 2022). These observations point to a regional phase of net incision and therefore landscape response to global climate change. For several of these locations, including the Toro Basin, local tectonic activity may have provided a secondary driver for incision, or created conditions conducive to fan/terrace preservation. Towards the Andean interior, the geomorphic response to the MPT probably lessens, as moisture and the extent of past glaciations is



732 more restricted (Luna et al., 2018; Haselton et al., 2002). Beyond the Central Andes, fluvial terraces
733 along the Río Deseado (47°S) (Tobal et al., 2021) and Río Santa Cruz (50°S) (Milanez Fernandes,
734 2023), draining the Southern Andes in Patagonia also record a period of net incision that can be
735 tentatively linked to the MPT. On a global scale, a growing number of studies have identified periods
736 of intensified erosion at this time, for example in the St. Elias mountains, Alaska (Gulick et al., 2015),
737 Central Appalachia (Del Vecchio et al., 2022), the Rocky Mountains (Pederson and Egholm, 2013) and
738 the European Alps (Haeuselmann et al., 2007; Valla et al., 2011; Sternai et al., 2013). While it is not
739 possible to discount a tectonic influence on landscape change in the upper Toro basin entirely, the links
740 between MPT climate and incision, and its expression elsewhere in the Andes and beyond, is
741 compelling.
742



743
744 **Figure 9.** Correlation between recorded climate cyclicity and upstream river length recognised in four basins of the Central
745 Andes (Fisher et al., 2016; Schildgen et al., 2016; Tofelde et al., 2017; D'Arcy et al. 2018; this study). Adapted from Tofelde
746 et al. (2017). Recorded period: $0.019 \times \text{river length}^2$.
747

748 5.4 Climate periodicity and alluvial channel system length

749 Higher frequency climate cycles are recorded in fan generation G2 of the Sierra de Pascha tributaries
750 compared with the mainstem of the basin; the alluvial fans, which appear to record climate cycles with
751 a periodicity of ca. 20 to 40-kyr have an upstream channel length of ~10 km and are positioned ~30 km
752 upstream of the terrace sequence showing 100-kyr climate cyclicity dated by Tofelde et al. (2017). This
753 finding substantiates the theory that the response time of alluvial channel systems to perturbations in
754 climate depends on system length (Paola et al., 1992; Castelltort and Van Den Driessche, 2003; Godard
755 et al., 2013; McNab et al., 2023). Evidence of this relationship, together with the dependency on the
756 square of the system length, was identified in the archive of several sedimentary basins in the Central
757 Andes, although only a single forcing frequency was recorded within each basin (Fig. 9) (Tofelde et al.,
758 2017). Our new data from the Toro Basin provide critical field evidence that multiple climate



periodicities can be preserved within the sedimentary record of a single sedimentary basin, with higher forcing frequencies recorded only in the uppermost reaches of the basin.

6. Conclusions

The alluvial fan and terrace sequences of the Toro basin present an excellent opportunity to explore (1) how channel responses to external perturbations may or may not propagate downstream, and (2) the differences in landscape response to forcing frequency as a function of stream length. We applied CRN dating to a suite of alluvial fan surfaces to characterise the evolution of the alluvial channel network of the Toro basin over the last one million years. Our key findings are as follows:

1. We identified two generations of fan surfaces (G1 and G2) were identified in the Sierra de Pascha tributary catchments. The G1 fans record CRN exposure (^{10}Be) ages between ca. 800 and 500 ka, whereas the G2 fans record surface activity and then abandonment between ca. 100 and 20 ka.
2. The G1 fans capture a significant phase of net incision (~ 200 m) between ca. 800 and 500 ka. The stepwise evacuation of the upper basin coincides with the onset of prolonged and enhanced global glacial cycles following the Mid-Pleistocene Transition (MPT). With several basins in the Central Andes and beyond also registering this phase of incision, we propose that the G1 fans are part of a continental scale response to MPT climate change.
3. The abandonment of the G2 fans is restricted to glacial periods, mostly modulated by 21/40-kyr climate cycles; enhanced moisture availability due to an intensified SASM likely amplified channel incision and sediment transport.
4. Differences in the timing of alluvial fan and fluvial terrace development in the upper and lower Toro basins appear to be associated with how channel length affects fluvial response time to climate forcing as well as local controls on net incision, which facilitates preservation of the geomorphic record of aggradation-incision cycles.
5. The new alluvial fan record from the upper Toro Basin, combined with earlier results on fluvial terraces from the lower Toro Basin, provides field evidence for the theoretical predictions of a scaling relationship between climate forcing frequency recorded in sedimentary archives and the system length. We show that multiple climate periodicities can be preserved within the sedimentary record of a single sedimentary basin, with higher forcing frequencies recorded only in the uppermost reaches of the basin. This improved understanding of the role of system length in climate signal propagation is an important step forward in helping us to anticipate the spatial distribution of sedimentary paleoclimate records within landscapes.



7. Code/data availability

All data is included as part of the manuscript.

8. Author contribution

Conceptualization: E.N.O, T.F.S, S.T; Sample collection and processing: E.N.O, T.F.S, S.T, H.W.;

Visualization: E.N.O with feedback from all authors; Writing & editing: all authors.

9. Competing interests

The authors declare that they have no conflict of interest.

10. Acknowledgments

This work was co-funded by (1) the German Research Foundation (DFG) grant 373/34-1 and the Brandenburg Ministry of Sciences, Research, and Cultural Affairs, within the framework of the International Research Training Group IGK2018 SuRfAce processes, TEctonics and Georesources: The Andean foreland basin of Argentina (StRATEGy) and (2) the European Research Council (ERC) under the European Union's Horizon 2020 Research and Innovation program (ERC Consolidator Grant 863490 to T.F.S.). TanDEM-X 12-m resolution digital elevation data were provided by the German Aerospace Center (DLR) through grant DEM_GEOL1915 to T.F. S. We thank Yanina Rojo for logistical support leading up to and during all field work. We also thank Peter van der Beek for assistance during field work.

11. References

- Armitage, J.J., Dunkley Jones, T., Duller, R.A., Whittaker, A.C., Allen, P.A. Temporal buffering of climate-driven sediment flux cycles by transient catchment response. *Earth and Planetary Science Letters*, 369–370, 200–210. <https://doi.org/10.1016/j.epsl.2013.03.020>, 2013.
- Baker, P.A., Rigsby, C.A., Seltzer, G.O., Fritz, S.C., Lowenstein, T.K., Bacher, N.P., Veliz, C. Tropical climate changes at millennial and orbital timescales on the Bolivian Altiplano. *Nature*, 409(6821), 698–701. <https://doi.org/10.1038/35055524>, 2001.
- Baker, P.A., Fritz, S.C. Nature and causes of Quaternary climate variation of tropical South America. *Quaternary Science Reviews*, 124, 31–47. <https://doi.org/10.1016/j.quascirev.2015.06.011>, 2015.
- Berger, A., Li, X.S., Loutre, M.F. Modelling northern hemisphere ice volume over the last 3 Ma. *Quaternary Science Reviews*, 18(1), 1–11. [https://doi.org/10.1016/S0277-3791\(98\)00033-X](https://doi.org/10.1016/S0277-3791(98)00033-X), 1999.
- Berger, A., Loutre, M.F. Insolation values for the climate of the last 10 million years. *Quaternary Science Reviews*, 10(4), 297–317. [https://doi.org/10.1016/0277-3791\(91\)90033-Q](https://doi.org/10.1016/0277-3791(91)90033-Q), 1991.
- Bernard, T., Sinclair, H.D., Gailleton, B., Mudd, S.M., Ford, M. Lithological control on the post-orogenic topography and erosion history of the Pyrenees. *Earth and Planetary Science Letters*, 518, 53–66. <https://doi.org/10.1016/j.epsl.2019.04.034>, 2019.
- Blard, P.-H., Braucher, R., Lavé, J., Bourlès, D. Cosmogenic ^{10}Be production rate calibrated against ^3He in the high Tropical Andes (3800–4900 m, 20–22° S). *Earth and Planetary Science Letters*, 382, 140–149. <https://doi.org/10.1016/j.epsl.2013.09.010>, 2013.
- Bobst, A.L., Lowenstein, T.K., Jordan, T.E., Godfrey, L.V., Ku, T.L., Luo, S. A 106 ka paleoclimate record from drill core of the Salar de Atacama, northern Chile. *Palaeogeography, Palaeoclimatology, Palaeoecology*, 173(1–2), 21–42. [https://doi.org/10.1016/S0031-0182\(01\)00308-X](https://doi.org/10.1016/S0031-0182(01)00308-X), 2001.
- Bonorino, G.G., Abascal, L. Drainage and base-level adjustments during evolution of a late Pleistocene piggyback basin, Eastern Cordillera, Central Andes of northwestern Argentina. *Bulletin*, 124(11–12), 1858–1870. <https://doi.org/10.1130/B30395.1>, 2012.
- Bookhagen, B., Strecker, M.R. Orographic barriers, high-resolution TRMM rainfall, and relief variations along the eastern Andes. *Geophysical Research Letters*, 35. <https://doi.org/10.1029/2007GL032011>, 2008.



- 849 Brocard, G., Willenbring, J., Suski, B., Audra, P., Authemayou, C., Cosenza-Murales, B., Morán-Ical,
850 S., Demory, F., Rochette, P., Vennemann, T., Holliger, K. Rate and processes of river network
851 rearrangement during incipient faulting: The case of the Cahabón River, Guatemala. *American*
852 *Journal of Science*, 312(5), 449-507, <https://doi.org/10.2475/05.2012.01>, 2012.
- 853 Broccoli, A.J., Dahl, K.A., Stouffer, R.J. Response of the ITCZ to Northern Hemisphere cooling.
854 *Geophysical Research Letters*, 33(1). <https://doi.org/10.1029/2005GL024546>, 2006.
- 855 Brooke, S.A., Whittaker, A.C., Armitage, J.J., D'Arcy, M., Watkins, S.E. Quantifying sediment
856 transport dynamics on alluvial fans from spatial and temporal changes in grain size, Death
857 Valley, California. *Journal of Geophysical Research: Earth Surface*, 123(8), 2039-2067.
858 <https://doi.org/10.1029/2018JF004622>, 2018.
- 859 Bufer, A., Burbank, D.W., Liu, L., Bookhagen, B., Qin, J., Chen, J., Li, T., Thompson Jobe, J.A., Yang,
860 H. Variations of lateral bedrock erosion rates control planation of uplifting folds in the foreland
861 of the Tian Shan, NW China. *Journal of Geophysical Research: Earth Surface*, 122(12), 2431-
862 2467. <https://doi.org/10.1002/2016JF004099>, 2017.
- 863 Buter, A., Heckmann, T., Filisetti, L., Savi, S., Mao, L., Gems, B., Comiti, F. Effects of catchment
864 characteristics and hydro-meteorological scenarios on sediment connectivity in glacierised
865 catchments. *Geomorphology*, 402, 108128. <https://doi.org/10.1016/j.geomorph.2022.108128>,
866 2022.
- 867 Castelltort, S., Van Den Driessche, J. How plausible are high-frequency sediment supply-driven cycles
868 in the stratigraphic record? *Sedimentary Geology*, 157, 3–13. [https://doi.org/10.1016/S0037-0738\(03\)00066-6](https://doi.org/10.1016/S0037-0738(03)00066-6), 2003.
- 870 Castino, F., Bookhagen, B., Strecker, M.R. Rainfall variability and trends of the past six decades (1950–
871 2014) in the subtropical NW Argentine Andes. *Climate Dynamics*, 48, 1049-1067.
872 <https://doi.org/10.1007/s00382-016-3127-2>, 2017.
- 873 Cesta, J.M., Ward, D.J. Timing and nature of alluvial fan development along the Chajnantor Plateau,
874 northern Chile. *Geomorphology*, 273, 412–427.
875 <https://doi.org/10.1016/j.geomorph.2016.09.003>, 2016.
- 876 Clarke, L., Quine, T.A., Nicholas, A. An experimental investigation of autogenic behaviour during
877 alluvial fan evolution. *Geomorphology*, 115(3-4), 278-285.
878 <https://doi.org/10.1016/j.geomorph.2009.06.033>, 2010.
- 879 Counts, R.C., Murari, M.K., Owen, L.A., Mahan, S.A., Greenan, M. Late Quaternary
880 chronostratigraphic framework of terraces and alluvium along the lower Ohio River,
881 southwestern Indiana and western Kentucky, USA. *Quaternary Science Reviews*, 110, 72-91.
882 <https://doi.org/10.1016/j.quascirev.2014.11.011>, 2015.
- 883 Crivellari, S., Chiessi, C.M., Kuhnert, H., Häggi, C., da Costa Portilho-Ramos, R., Zeng, J.Y., Zhang,
884 Y., Schefuß, E., Mollenhauer, G., Hefter, J., Alexandre, F. Increased Amazon freshwater
885 discharge during late Heinrich Stadial 1. *Quaternary Science Reviews*, 181, 144-155.
886 <https://doi.org/10.1016/j.quascirev.2017.12.005>, 2018.
- 887 D'Arcy, M.K., Schildgen, T.F., Strecker, M.R., Wittmann, H., Duesing, W., Mey, J., Tofelde, S.,
888 Weissmann, P., Alonso, R.N. Timing of past glaciation at the Sierra de Aconquija, northwestern
889 Argentina, and throughout the Central Andes. *Quaternary Science Reviews*, 204, 37–57.
890 <https://doi.org/10.1016/j.quascirev.2018.11.022>, 2019a.
- 891 D'Arcy, M.K., Schildgen, T.F., Turowski, J.M., Dinezio, P. Inferring the timing of abandonment of
892 aggraded alluvial surfaces dated with cosmogenic nuclides. *Earth Surface Dynamics*, 7, 755–
893 771. <https://doi.org/10.5194/esurf-7-755-2019>, 2019b.
- 894 D'Arcy, M., Schildgen, T.F., Tofelde, S., Strecker, M.R., Wittmann, H., Düsing, W., Weissmann, P.
895 and Roda-Boluda, D.C. Catchment-alluvial fan systems record > 200 ka of millennial-scale
896 climate changes in the subtropical Andes. *EGU General Assembly Conference Abstracts*.
897 <https://ui.adsabs.harvard.edu/abs/2018EGUGA..20.4710D/abstract>, 2018.
- 898 DeCelles, P.G., Carrapa, B., Horton, B.K., Gehrels, G.E. Cenozoic foreland basin system in the central
899 Andes of northwestern Argentina: Implications for Andean geodynamics and modes of
900 deformation. *Tectonics*, 30(6). <https://doi.org/10.1029/2011TC002948>, 2011.
- 901 Del Vecchio, J., DiBiase, R.A., Corbett, L.B., Bierman, P.R., Caffee, M.W., Ivory, S.J. Increased
902 erosion rates following the onset of Pleistocene periglacialiation at Bear Meadows, Pennsylvania,



- 903 USA. Geophysical Research Letters, 49(4), p.e2021GL096739.
- 904 <https://doi.org/10.1029/2021GL096739>, 2022.
- 905 Dey, S., Thiede, R.C., Schildgen, T.F., Wittmann, H., Bookhagen, B., Scherler, D., Jain, V., Strecker,
- 906 M.R. Climate-driven sediment aggradation and incision since the late Pleistocene in the NW
- 907 Himalaya, India. Earth and Planetary Science Letters, 449, 321–331.
- 908 <https://doi.org/10.1016/j.epsl.2016.05.050>, 2016.
- 909 Dortch, J.M., Tomkins, M.D., Saha, S., Murari, M.K., Schoenbohm, L.M., Curl, D. A tool for the ages:
- 910 The Probabilistic Cosmogenic Age Analysis Tool (P-CAAT). Quaternary Geochronology, 71,
- 911 101323. <https://doi.org/10.1016/j.quageo.2022.101323>, 2022.
- 912 Dühnforth, M., Densmore, A.L., Ivy-Ochs, S., Allen, P., Kubik, P.W. Early to Late Pleistocene history
- 913 of debris-flow fan evolution in western Death Valley (California) using cosmogenic ^{10}Be and
- 914 ^{26}Al . Geomorphology, 281, 53–65. <https://doi.org/10.1016/j.geomorph.2016.12.020>, 2017.
- 915 Dühnforth, M., Densmore, A.L., Ivy-Ochs, S., Allen, P.A., Kubik, P.W. Timing and patterns of debris
- 916 flow deposition on Shepherd and Symmes creek fans, Owens Valley, California, deduced from
- 917 cosmogenic ^{10}Be . Journal of Geophysical Research: Earth Surface, 112.
- 918 <https://doi.org/10.1029/2006JF000562>, 2007.
- 919 Dunai, T.J., López, G.A.G., Juez-Larré, J. Oligocene–Miocene age of aridity in the Atacama Desert
- 920 revealed by exposure dating of erosion-sensitive landforms. Geology, 33(4), 321–324.
- 921 <https://doi.org/10.1130/G21184.1>, 2005.
- 922 Fernandes, V.M., Schildgen, T., Ruby, A., Wittmann-Oelze, H., McNab, F. Pleistocene Landscape
- 923 Evolution in Southern Patagonia: A Record of Regional Incision from ^{10}Be Dating of Fluvial
- 924 Terraces (No. EGU23-15938). Copernicus Meetings. [https://doi.org/10.5194/egusphere-](https://doi.org/10.5194/egusphere-egu23-15938)
- 925 [egu23-15938](https://doi.org/10.5194/egusphere-egu23-15938), 2023.
- 926 Fisher, G.B., Luna, L.V., Amidon, W.H., Burbank, D.W., de Boer, B., Stap, L.B., Bookhagen, B.,
- 927 Godard, V., Oskin, M.E., Alonso, R.N., and Tuenter, E. Milankovitch-paced erosion in the
- 928 southern Central Andes. Nature Communications, 14(1), 424 [https://doi.org/10.1038/s41467-](https://doi.org/10.1038/s41467-023-36022-0)
- 929 [023-36022-0](https://doi.org/10.1038/s41467-023-36022-0), 2023.
- 930 Fritz, S.C., Baker, P.A., Ekdahl, E., Seltzer, G.O., Stevens, L.R. Millennial-scale climate variability
- 931 during the Last Glacial period in the tropical Andes. Quaternary Science Reviews, 29(7-8),
- 932 1017–1024. <https://doi.org/10.1016/j.quascirev.2010.01.001>, 2010.
- 933 Fritz, S.C., Baker, P.A., Seltzer, G.O., Ballantyne, A., Tapia, P., Cheng, H., Edwards, R.L. Quaternary
- 934 glaciation and hydrologic variation in the South American tropics as reconstructed from the
- 935 Lake Titicaca drilling project. Quaternary Research, 68(3), 410–420.
- 936 <https://doi.org/10.1016/j.yqres.2007.07.008>, 2007.
- 937 Fritz, S.C., Baker, P.A., Lowenstein, T.K., Seltzer, G.O., Rigsby, C.A., Dwyer, G.S., Tapia, P.M.,
- 938 Arnold, K.K., Ku, T.L., Luo, S. Hydrologic variation during the last 170,000 years in the
- 939 southern hemisphere tropics of South America. Quaternary Research, 61(1), 95–104.
- 940 <https://doi.org/10.1016/j.yqres.2003.08.007>, 2004.
- 941 Fryirs, K.A., Brierley, G.J., Preston, N.J., Kasai, M. Buffers, barriers and blankets: The (dis)
- 942 connectivity of catchment-scale sediment cascades. Catena, 70(1), 49–67.
- 943 <https://doi.org/10.1016/j.catena.2006.07.007>, 2007.
- 944 Ganey, P.N., Dolan, J.F., Frankel, K.L., Finkel, R.C. Rates of extension along the Fish Lake Valley
- 945 fault and transtensional deformation in the Eastern California shear zone–Walker Lane belt.
- 946 Lithosphere, 2(1), 33–49. <https://doi.org/10.1130/L51.1>, 2010.
- 947 García, V.H., Hongn, F., Cristallini, E.O. Late Miocene to recent morphotectonic evolution and
- 948 potential seismic hazard of the northern Lerma valley: clues from Lomas de Medeiros,
- 949 Cordillera Oriental, NW Argentina. Tectonophysics, 608, 1238–1253.
- 950 <https://doi.org/10.1016/j.tecto.2013.06.021>, 2013.
- 951 Godard, V., Tucker, G.E., Burch Fisher, G., Burbank, D.W., Bookhagen, B. Frequency-dependent
- 952 landscape response to climatic forcing. Geophysical Research Letters, 40, 859–863.
- 953 <https://doi.org/10.1002/grl.50253>, 2013.
- 954 Godfrey, L.V., Jordan, T.E., Lowenstein, T.K., Alonso, R.L. Stable isotope constraints on the transport
- 955 of water to the Andes between 22 and 26 S during the last glacial cycle. Palaeogeography,
- 956 Palaeoclimatology, Palaeoecology, 194(1-3), 299–317. [https://doi.org/10.1016/S0031-](https://doi.org/10.1016/S0031-0182(03)00283-9)
- 957 [0182\(03\)00283-9](https://doi.org/10.1016/S0031-0182(03)00283-9), 2003.



- 1958 Gosling, W.D., Bush, M.B., Hanselman, J.A., Chepstow-Lusty, A. Glacial-interglacial changes in
1959 moisture balance and the impact on vegetation in the southern hemisphere tropical Andes
1960 (Bolivia/Peru). *Palaeogeography, Palaeoclimatology, Palaeoecology*, 259(1), 35-50.
1961 <https://doi.org/10.1016/j.palaeo.2007.02.050>, 2008.
- 1962 Gray, H.J., Owen, L.A., Dietsch, C., Beck, R.A., Caffee, M.A., Finkel, R.C., Mahan, S.A. Quaternary
1963 landscape development, alluvial fan chronology and erosion of the Mecca Hills at the southern
1964 end of the San Andreas fault zone. *Quaternary Science Reviews*, 105, 66-85.
1965 <https://doi.org/10.1016/j.quascirev.2014.09.009>, 2014.
- 1966 Guarnieri, P., Pirrotta, C. The response of drainage basins to the late Quaternary tectonics in the Sicilian
1967 side of the Messina Strait (NE Sicily). *Geomorphology*, 95(3-4), 260-273.
1968 <https://doi.org/10.1016/j.geomorph.2007.06.013>, 2008.
- 1969 Gulick, S.P., Jaeger, J.M., Mix, A.C., Asahi, H., Bahlburg, H., Belanger, C.L., Berbel, G.B., Childress,
1970 L., Cowan, E., Drab, L., Forwick, M. Mid-Pleistocene climate transition drives net mass loss
1971 from rapidly uplifting St. Elias Mountains, Alaska. *Proceedings of the National Academy of*
1972 *Sciences*, 112(49), 15042-15047. <https://doi.org/10.1073/pnas.1512549112>, 2015.
- 1973 Haeuselmann, P., Granger, D.E., Jeannin, P.Y., Lauritzen, S.E. Abrupt glacial valley incision at 0.8 Ma
1974 dated from cave deposits in Switzerland. *Geology*, 35(2), 143-146.
1975 <https://doi.org/10.1130/G23094A>, 2007.
- 1976 Hain, M.P., Strecker, M.R., Bookhagen, B., Alonso, R.N., Pingel, H., Schmitt, A.K. Neogene to
1977 Quaternary broken foreland formation and sedimentation dynamics in the Andes of NW
1978 Argentina (25 S). *Tectonics*, 30(2). <https://doi.org/10.1029/2010TC002703>, 2011.
- 1979 Harvey, A.M. The coupling status of alluvial fans and debris cones: a review and synthesis. *Earth*
1980 *Surface Processes and Landforms*, 37(1), 64-76. <https://doi.org/10.1002/esp.2213>, 2012.
- 1981 Harvey, A.M., Silva, P.G., Mather, A.E., Goy, J.L., Stokes, M., Zazo, C. The impact of Quaternary sea-
1982 level and climatic change on coastal alluvial fans in the Cabo de Gata ranges, southeast Spain.
1983 *Geomorphology*, 28(1-2), 1-22 [https://doi.org/10.1016/S0169-555X\(98\)00100-7](https://doi.org/10.1016/S0169-555X(98)00100-7), 1999.
- 1984 Haselton, K., Hilley, G., Strecker, M.R. Average Pleistocene climatic patterns in the southern central
1985 Andes: Controls on mountain glaciation and paleoclimate implications. *The Journal of*
1986 *Geology*, 110(2), 211-226. 2002.
- 1987 Hedrick, K., Owen, L.A., Rockwell, T.K., Meigs, A., Costa, C., Caffee, M.W., Masana, E., Ahumada,
1988 E. Timing and nature of alluvial fan and strath terrace formation in the Eastern Precordillera of
1989 Argentina. *Quaternary Science Reviews*, 80, 143-168
1990 <https://doi.org/10.1016/j.quascirev.2013.05.004>, 2013.
- 1991 Hidy, A.J., Gosse, J.C., Pederson, J.L., Mattern, J.P., Finkel, R.C. A geologically constrained Monte
1992 Carlo approach to modeling exposure ages from profiles of cosmogenic nuclides: An example
1993 from Lees Ferry, Arizona. *Geochemistry Geophysics Geosystems*, 11, Q0AA10.
1994 <https://doi.org/10.1029/2010GC003084>, 2010.
- 1995 Hilley, G.E., Strecker, M.R. Processes of oscillatory basin filling and excavation in a tectonically active
1996 orogen: Quebrada del Toro Basin, NW Argentina. *Bulletin of the Geological Society of*
1997 *America*, 117, 887-901. <https://doi.org/10.1130/B25602.1>, 2005.
- 1998 Howard, A.D. Equilibrium and time scales in geomorphology: Application to sand-bed alluvial streams.
1999 *Earth Surface Processes and Landforms*, 7(4), pp.303-325.
1000 <https://doi.org/10.1002/esp.3290070403>, 1982.
- 1001 Hughes, P.D. Geomorphology and Quaternary stratigraphy: The roles of morpho-, litho-, and
1002 allostratigraphy. *Geomorphology*, 123, 189-199.
1003 <https://doi.org/10.1016/j.geomorph.2010.07.025>, 2010.
- 1004 Imbrie, John., McIntyre, Andrew. SST vs time for core V25-21 (specmap.059). PANGAEA., 2006.
- 1005 Kelly, M.A., Lowell, T. V., Applegate, P.J., Phillips, F.M., Schaefer, J.M., Smith, C.A., Kim, H.,
1006 Leonard, K.C., Hudson, A.M. A locally calibrated, late glacial ¹⁰Be production rate from a low-
1007 latitude, high-altitude site in the Peruvian Andes. *Quaternary Geochronology*, 26, 70-85.
1008 <https://doi.org/10.1016/j.quageo.2013.10.007>, 2015.
- 1009 Kleinert, K., Strecker, M.R. Climate change in response to orographic barrier uplift: Paleosol and stable
1010 isotope evidence from the late Neogene Santa Maria basin, northwestern Argentina. *Geological*
1011 *Society of America Bulletin*, 113(6), 728-742. [https://doi.org/10.1130/0016-7606\(2001\)113<0728:CCIRTO>2.0.CO;2](https://doi.org/10.1130/0016-7606(2001)113<0728:CCIRTO>2.0.CO;2), 2001.
- 1012



- 1013 Kober, F., Zeilinger, G., Ivy-Ochs, S., Dolati, A., Smit, J., Kubik, P.W. Climatic and tectonic control
1014 on fluvial and alluvial fan sequence formation in the Central Makran Range, SE-Iran. *Global*
1015 *and Planetary Change*, 111, 133-149. <https://doi.org/10.1016/j.gloplacha.2013.09.003>, 2013.
- 1016 Lal, D. Cosmic ray labeling of erosion surfaces: in situ nuclide production rates and erosion models.
1017 *Earth and Planetary Science Letters*, 104, 424–439. [https://doi.org/10.1016/0012-](https://doi.org/10.1016/0012-821X(91)90220-C)
1018 [821X\(91\)90220-C](https://doi.org/10.1016/0012-821X(91)90220-C), 1991.
- 1019 Lifton, N., Sato, T., Dunai, T.J. Scaling in situ cosmogenic nuclide production rates using analytical
1020 approximations to atmospheric cosmic-ray fluxes. *Earth and Planetary Science Letters*, 386,
1021 149–160. <https://doi.org/10.1016/j.epsl.2013.10.052>, 2014.
- 1022 Lisiecki, L.E., Raymo, M.E. Diachronous benthic $\delta^{18}\text{O}$ responses during late Pleistocene terminations.
1023 *Paleoceanography*, 24(3). <https://doi.org/10.1029/2009PA001732>, 2009.
- 1024 Luna, L. V., Bookhagen, B., Niedermann, S., Rugel, G., Scharf, A., Merchel, S. Glacial chronology and
1025 production rate cross-calibration of five cosmogenic nuclide and mineral systems from the
1026 southern Central Andean Plateau. *Earth and Planetary Science Letters*, 500, 242–253.
1027 <https://doi.org/10.1016/j.epsl.2018.07.034>, 2018.
- 1028 Ma, Y., Stuart, F.M. The use of in-situ cosmogenic ^{21}Ne in studies on long-term landscape development.
1029 *Acta Geochimica*, 37, 310-322. <https://doi.org/10.1007/s11631-017-0216-9>, 2018.
- 1030 Mackin, J. Concept of the graded river. *Geological Society of America Bulletin*, 59(5), 463-512, 1948.
- 1031 Malamud, B.D., Jordan, T.E., Alonso, R.A., Gallardo, E.F., Gonzalez, R.E., Kelley, S.A. Pleistocene
1032 Lake Lerma, Salta Province, NW Argentina. In XIII Congreso Geológico Argentino y III
1033 Congreso de Exploración de Hidrocarburos, Vol. 1, 103-114, 1996.
- 1034 Marrett, R., Strecker, M.R. Response of intracontinental deformation in the central Andes to late
1035 Cenozoic reorganization of South American Plate motions. *Tectonics*, 19(3), 452-467.
1036 <https://doi.org/10.1029/1999TC001102>, 2000.
- 1037 Marrett, R.A., Allmendinger, R.W., Alonso, R.N., Drake, R.E. Late Cenozoic tectonic evolution of the
1038 Puna Plateau and adjacent foreland, northwestern Argentine Andes. *Journal of South American*
1039 *Earth Sciences*, 7(2), 179-207. [https://doi.org/10.1016/0895-9811\(94\)90007-8](https://doi.org/10.1016/0895-9811(94)90007-8), 1994.
- 1040 Martin, L.C.P., Blard, P.-H., Balco, G., Lavé, J., Delunel, R., Lifton, N., Laurent, V. The CREP program
1041 and the ICE-D production rate calibration database: A fully parameterizable and updated online
1042 tool to compute cosmic-ray exposure ages. *Quaternary Geochronology*, 38, 25–49.
1043 <https://doi.org/10.1016/j.quageo.2016.11.006>, 2017.
- 1044 Martin, L.C.P., Blard, P.-H., Lavé, J., Braucher, R., Lupker, M., Condom, T., Charreau, J., Mariotti, V.,
1045 ASTER Team, Davy, E. In situ cosmogenic ^{10}Be production rate in the High Tropical Andes.
1046 *Quaternary Geochronology*, 30, 54–68. <https://doi.org/10.1016/j.quageo.2015.06.012>, 2015.
- 1047 Martin, L.C., Blard, P.H., Lavé, J., Condom, T., Prémaillon, M., Jomelli, V., Brunstein, D., Lupker, M.,
1048 Charreau, J., Mariotti, V., Tibari, B. Lake Tauca highstand (Heinrich Stadial 1a) driven by a
1049 southward shift of the Bolivian High. *Science Advances*, 4(8),
1050 <https://doi.org/10.1126/sciadv.aar2514>, 2018.
- 1051 Martini, M.A., Kaplan, M.R., Strelin, J.A., Astini, R.A., Schaefer, J.M., Caffee, M.W., Schwartz, R.
1052 Late Pleistocene glacial fluctuations in Cordillera oriental, subtropical Andes. *Quaternary*
1053 *Science Reviews*, 171, 245-259. <https://doi.org/10.1016/j.quascirev.2017.06.033>, 2017.
- 1054 Mather, A.E., Stokes, M., Whitfield, E. River terraces and alluvial fans: The case for an integrated
1055 Quaternary fluvial archive. *Quaternary Science Reviews* 166, 74-90,
1056 <https://doi.org/10.1016/j.quascirev.2016.09.022>, 2017.
- 1057 Mazzuoli, R., Vezzoli, L., Omarini, R., Acocella, V., Gioncada, A., Matteini, M., Dini, A., Guillou, H.,
1058 Hauser, N., Uttini, A., Scaillet, S. Miocene magmatism and tectonics of the easternmost sector
1059 of the Calama–Olacapato–El Toro fault system in Central Andes at ~ 24 S: Insights into the
1060 evolution of the Eastern Cordillera. *GSA Bulletin* 120(11-12), 1493-1517,
1061 <https://doi.org/10.1130/B26109.1>, 2008.
- 1062 McFadden, L.D., Ritter, J.B., Wells, S.G. Use of Multiparameter Relative-Age Methods for Age
1063 Estimation and Correlation of Alluvial Fan Surfaces on a Desert Piedmont, Eastern Mojave
1064 Desert, California. *Quaternary Research* 32, 276–290, [https://doi.org/10.1016/0033-](https://doi.org/10.1016/0033-5894(89)90094-X)
1065 [5894\(89\)90094-X](https://doi.org/10.1016/0033-5894(89)90094-X), 1989.



- 1066 McNab, F., Schildgen, T.F., Turowski, J.M., Wickert, A.D. Diverse responses of alluvial rivers to
1067 periodic environmental change. *Geophysical Research Letters* 50(10), e2023GL103075,
1068 <https://doi.org/10.1029/2023GL103075>, 2023.
- 1069 Mescolotti, P.C., do Nascimento Pupim, F., Ladeira, F.S.B., Sawakuchi, A.O., Santa Catharina, A.,
1070 Assine, M.L. Fluvial aggradation and incision in the Brazilian tropical semi-arid: Climate-
1071 controlled landscape evolution of the São Francisco River. *Quaternary Science Reviews* 263,
1072 106977, <https://doi.org/10.1016/j.quascirev.2021.106977>, 2021.
- 1073 Mey, J., D'Arcy, M.K., Schildgen, T.F., Egholm, D.L., Wittmann, H., Strecker, M.R. Temperature and
1074 precipitation in the southern Central Andes during the last glacial maximum, Heinrich Stadial
1075 1, and the Younger Dryas. *Quaternary Science Reviews* 248, 106592,
1076 <https://doi.org/10.1016/j.quascirev.2020.106592>, 2020.
- 1077 Mosblech, N.A., Bush, M.B., Gosling, W.D., Hodell, D., Thomas, L., Van Calsteren, P., Correa-Metrio,
1078 A., Valencia, B.G., Curtis, J., Van Woesik, R. North Atlantic forcing of Amazonian
1079 precipitation during the last ice age. *Nature Geoscience* 5(11), 817-820,
1080 <https://doi.org/10.1038/ngeo1588>, 2012.
- 1081 Mouchené, M., van der Beek, P., Carretier, S., Mouthereau, F. Autogenic versus allogenic controls on
1082 the evolution of a coupled fluvial megafan–mountainous catchment system: numerical
1083 modelling and comparison with the Lannemezan megafan system (northern Pyrenees, France).
1084 *Earth Surface Dynamics* 5(1), 125-143, <https://doi.org/10.5194/esurf-5-125-2017>, 2017.
- 1085 Mouslopoulou, V., Begg, J., Fülling, A., Moraetis, D., Partsinevelos, P., Oncken, O. Distinct phases of
1086 eustatic and tectonic forcing for late Quaternary landscape evolution in southwest Crete,
1087 Greece. *Earth Surface Dynamics* 5(3), 511-527, <https://doi.org/10.5194/esurf-5-511-2017>,
1088 2017.
- 1089 Nicholas, A.P., Quine, T.A. Modeling alluvial landform change in the absence of external
1090 environmental forcing. *Geology* 35(6), 527-530, <https://doi.org/10.1130/G23377A.1>, 2007.
- 1091 Nishiizumi, K., Winterer, E.L., Kohl, C.P., Klein, J., Middleton, R., Lal, D., Arnold, J.R. Cosmic ray
1092 production rates of ¹⁰Be and ²⁶Al in quartz from glacially polished rocks. *Journal of Geophysical*
1093 *Research* 94, 17907, <https://doi.org/10.1029/JB094iB12p17907>, 1989.
- 1094 Novello, V.F., Cruz, F.W., Vuille, M., Strikis, N.M., Edwards, R.L., Cheng, H., Emerick, S., De Paula,
1095 M.S., Li, X., Barreto, E.D.S., Karmann, I. A high-resolution history of the South American
1096 Monsoon from Last Glacial Maximum to the Holocene. *Scientific Reports* 7(1), 44267,
1097 <https://doi.org/10.1038/srep44267>, 2017.
- 1098 Orr, E.N., Owen, L.A., Saha, S., Caffee, M.W. Climate-driven late Quaternary fan surface abandonment
1099 in the NW Himalaya. In: *Untangling the Quaternary Period—A Legacy of Stephen C. Porter*.
1100 *Geological Society of America*, 63–80, [https://doi.org/10.1130/2020.2548\(04\)](https://doi.org/10.1130/2020.2548(04)), 2021.
- 1101 Owen, L.A., Clemmens, S.J., Finkel, R.C., Gray, H. Late Quaternary alluvial fans at the eastern end of
1102 the San Bernardino Mountains, Southern California. *Quaternary Science Reviews*, 87, 114-
1103 134. <https://doi.org/10.1016/j.quascirev.2014.01.003>, 2014.
- 1104 Paola, C., Heller, P.L., Angevine, C.L. The large-scale dynamics of grain-size variation in alluvial
1105 basins. I: theory. *Basin Research*. 4, 73-90. <https://doi.org/10.1111/j.1365-2117.1992.tb00145.x>, 1992.
- 1106 Pedersen, V.K., Egholm, D.L. Glaciations in response to climate variations preconditioned by evolving
1107 topography. *Nature*, 493(7431), 206-210. <https://doi.org/10.1038/nature11786>, 2013.
- 1108 Peri, V.G., Haghipour, N., Christl, M., Terrizzano, C., Kaveh-Firouz, A., Leiva, M.F., Pérez, P., Yamin,
1109 M., Barcelona, H., Burg, J.P. Quaternary landscape evolution in the Western Argentine
1110 Precordillera constrained by ¹⁰Be cosmogenic dating. *Geomorphology* 396,
1111 <https://doi.org/10.1016/j.geomorph.2021.107984>, 2022.
- 1112 Perron, J.T., Royden, L. An integral approach to bedrock river profile analysis. *Earth Surface Processes*
1113 *and Landforms*, 38(6), 570-576. <https://doi.org/10.1002/esp.3302>, 2013.
- 1114 Pingel, H., Strecker, M.R., Mulch, A., Alonso, R.N., Cottle, J., Rohrmann, A. Late Cenozoic
1115 topographic evolution of the Eastern Cordillera and Puna Plateau margin in the southern Central
1116 Andes (NW Argentina). *Earth and Planetary Science Letters* 535, 116112,
1117 <https://doi.org/10.1016/j.epsl.2020.116112>, 2020.
- 1118



- 1119 Pingel, H., Alonso, R.N., Altenberger, U., Cottle, J., Strecker, M.R. Miocene to Quaternary basin
1120 evolution at the southeastern Andean Plateau (Puna) margin (ca. 24°S lat, Northwestern
1121 Argentina). *Basin Research* 31, 808–826. <https://doi.org/10.1111/bre.12346>, 2019a.
- 1122 Pingel, H., Schildgen, T., Strecker, M.R., Wittmann, H. Pliocene–Pleistocene orographic control on
1123 denudation in northwest Argentina. *Geology* 47, 359–362. <https://doi.org/10.1130/G45800.1>,
1124 2019b.
- 1125 Pingel, H., Mulch, A., Alonso, R.N., Cottle, J., Hynek, S.A., Poletti, J., Rohrmann, A., Schmitt, A.K.,
1126 Stockli, D.F. and Strecker, M.R. Surface uplift and convective rainfall along the southern
1127 Central Andes (Angastaco Basin, NW Argentina). *Earth and Planetary Science Letters*, 440,
1128 33–42. <https://doi.org/10.1016/j.epsl.2016.02.009>, 2016.
- 1129 Pingel, H., Strecker, M.R., Alonso, R.N., Schmitt, A.K. Neotectonic basin and landscape evolution in
1130 the Eastern Cordillera of NW Argentina, Humahuaca Basin (~ 24 S). *Basin Research*, 25(5),
1131 554–573. <https://doi.org/10.1111/bre.12016>, 2013.
- 1132 Placzek, C., Quade, J., Patchett, P.J. Geochronology and stratigraphy of late Pleistocene lake cycles on
1133 the southern Bolivian Altiplano: implications for causes of tropical climate change. *Geological*
1134 *Society of America Bulletin*, 118(5–6), 515–532. <https://doi.org/10.1130/B25770.1>, 2006.
- 1135 Prush, V.B., Oskin, M.E. A mechanistic erosion model for cosmogenic nuclide inheritance in single-
1136 clast exposure ages. *Earth and Planetary Science Letters* 535, 116066.
1137 <https://doi.org/10.1016/j.epsl.2020.116066>, 2020.
- 1138 Ratnayaka, K., Hetzel, R., Hornung, J., Hampel, A., Hinderer, M., Frechen, M. Postglacial alluvial fan
1139 dynamics in the Cordillera Oriental, Peru, and palaeoclimatic implications. *Quaternary*
1140 *Research*, 91, 431–449. <https://doi.org/10.1017/qua.2018.106>, 2019.
- 1141 Robinson, R.A.J., Spencer, J.Q.G., Strecker, M.R., Richter, A., Alonso, R.N. Luminescence dating of
1142 alluvial fans in intramontane basins of NW Argentina. In: Harvey, A.M. et. al, eds. *Alluvial*
1143 *Fans: Geomorphology, Sedimentology, Dynamics*. Geological Society. Special Publication
1144 251, 153–168. 2005.
- 1145 Robledo Juan M., Luisa M. Anzotegui, Olga G. Martínez., Ricardo N. Alonso. Flora and insect trace
1146 fossils from the Mio-Pliocene Quebrada del Toro locality (Gobernador Solá, Salta,
1147 Argentina). *Journal of South American Earth Sciences*, Volume 100, June 2020, 102544.
1148 <https://doi.org/10.1016/j.jsames.2020.102544>, 2020.
- 1149 Rohais, S., Bonnet, S. and Eschard, R. Sedimentary record of tectonic and climatic erosional
1150 perturbations in an experimental coupled catchment-fan system. *Basin Research*, 24(2), 198–
1151 212. <https://doi.org/10.1111/j.1365-2117.2011.00520.x>, 2012.
- 1152 Savi, S., Tofelde, S., Wickert, A.D., Bufo, A., Schildgen, T.F., Strecker, M.R. Interactions between
1153 main channels and tributary alluvial fans: channel adjustments and sediment-signal
1154 propagation. *Earth Surface Dynamics*, 8(2), 303–322. [https://doi.org/10.5194/esurf-8-303-
1155 2020](https://doi.org/10.5194/esurf-8-303-2020), 2020.
- 1156 Savi, S., Schildgen, T.F., Tofelde, S., Wittmann, H., Scherler, D., Mey, J., Alonso, R.N., Strecker, M.R.
1157 Climatic controls on debris-flow activity and sediment aggradation: The Del Medio fan, NW
1158 Argentina. *Journal of Geophysical Research: Earth Surface* 121, 2424–2445.
1159 <https://doi.org/10.1002/2016JF003912>, 2016.
- 1160 Schildgen, T.F., Robinson, R.A.J., Savi, S., Phillips, W.M., Spencer, J.Q.G., Bookhagen, B., Scherler,
1161 D., Tofelde, S., Alonso, R.N., Kubik, P.W., Binnie, S.A., Strecker, M.R. Landscape response
1162 to late Pleistocene climate change in NW Argentina: Sediment flux modulated by basin
1163 geometry and connectivity. *Journal of Geophysical Research: Earth Surface* 121, 392–414.
1164 <https://doi.org/10.1002/2015JF003607>, 2016.
- 1165 Schwab, K., Schäfer, A. Sedimentation und Tektonik im mittleren Abschnitt des Río Toro in der
1166 Ostkordillere NW-Argentinien. *Geologische Rundschau*, 65, 175–194.
1167 <https://doi.org/10.1007/BF01808462>, 1976.
- 1168 Schwanghart, W., Scherler, D. Short Communication: TopoToolbox 2 – MATLAB-based software for
1169 topographic analysis and modeling in Earth surface sciences. *Earth Surface Dynamics* 2, 1–7.
1170 <https://doi.org/10.5194/esurf-2-1-2014>, 2014.
- 1171 Simpson, G., Castelltort, S. Model shows that rivers transmit high-frequency climate cycles to the
1172 sedimentary record. *Geology* 40, 1131–1134. <https://doi.org/10.1130/G33451.1>, 2012.



- 1173 Seagren, E.G., Schoenbohm, L.M. Drainage reorganization across the Puna Plateau margin (NW
1174 Argentina): Implications for the preservation of orogenic plateaus. *Journal of Geophysical*
1175 *Research: Earth Surface*, 126(8), p.e2021JF006147. <https://doi.org/10.1029/2021JF006147>,
1176 2021.
- 1177 Seagren, E.G., McMillan, M., Schoenbohm, L.M. Tectonic control on drainage evolution in broken
1178 forelands: Examples from NW Argentina. *Tectonics*, 41(1), p.e2020TC006536,
1179 <https://doi.org/10.1029/2020TC006536>, 2022.
- 1180 Spelz, R.M., Fletcher, J.M., Owen, L.A. and Caffee, M.W. Quaternary alluvial-fan development,
1181 climate and morphologic dating of fault scarps in Laguna Salada, Baja California,
1182 Mexico. *Geomorphology*, 102(3-4), 578-594.
1183 <https://doi.org/10.1016/j.geomorph.2008.06.001>, 2008.
- 1184 Steffen, D., Schlunegger, F., Preusser, F. Late Pleistocene fans and terraces in the Majes valley,
1185 southern Peru, and their relation to climatic variations. *International Journal of Earth*
1186 *Sciences*, 99, 1975-1989. <https://doi.org/10.1007/s00531-009-0489-2>, 2010.
- 1187 Sternai, P., Herman, F., Valla, P.G., Champagnac, J.D. Spatial and temporal variations of glacial erosion
1188 in the Rhône valley (Swiss Alps): Insights from numerical modeling. *Earth and Planetary*
1189 *Science Letters* 368, 119–131. <https://doi.org/10.1016/j.epsl.2013.02.039>, 2013.
- 1190 Stone, J.O. Air pressure and cosmogenic isotope production. *Journal of Geophysical Research: Solid*
1191 *Earth* 105, 23753–23759. 2000.
- 1192 Strecker, M.R., Alonso, R., Bookhagen, B., Carrapa, B., Coutand, I., Hain, M.P., Hilley, G.E.,
1193 Mortimer, E., Schoenbohm, L., Sobel, E.R., 2009. Does the topographic distribution of the
1194 central Andean Puna Plateau result from climatic or geodynamic processes? *Geology*, 37(7),
1195 643-646. <https://doi.org/10.1130/G25545A.1>, 2009.
- 1196 Streit, R.L., Burbank, D.W., Strecker, M.R., Alonso, R.N., Cottle, J.M., Kylander-Clark, A.R.C.
1197 Controls on intermontane basin filling, isolation and incision on the margin of the Puna Plateau,
1198 NW Argentina (~23°S). *Basin Research* 29, 131–155. <https://doi.org/10.1111/bre.12141>, 2017.
- 1199 Terrizzano, C.M., García Morabito, E., Christl, M., Likerman, J., Tobal, J., Yamin, M., Zech, R.
1200 Climatic and Tectonic forcing on alluvial fans in the Southern Central Andes. *Quaternary*
1201 *Science Reviews* 172, 131–141. <https://doi.org/10.1016/j.quascirev.2017.08.002>, 2017.
- 1202 Tobal, J.E., Morabito, E.G., Terrizzano, C.M., Zech, R., Colavitto, B., Struck, J., Christl, M., Ghiglione,
1203 M.C. Quaternary landscape evolution of Patagonia at the Chilean Triple Junction: Climate and
1204 tectonic forcings. *Quaternary Science Reviews*, 261, 106960.
1205 <https://doi.org/10.1016/j.quascirev.2021.106960>, 2021.
- 1206 Tofelde, S., Duesing, W., Schildgen, T.F., Wickert, A.D., Wittmann, H., Alonso, R.N., Strecker, M.
1207 Effects of deep-seated versus shallow hillslope processes on cosmogenic ¹⁰Be concentrations
1208 in fluvial sand and gravel. *Earth Surface Processes and Landforms* 43, 3086–3098.
1209 <https://doi.org/10.1002/esp.4471>, 2018.
- 1210 Tofelde, S., Savi, S., Wickert, A.D., Bufo, A., Schildgen, T.F. Alluvial channel response to
1211 environmental perturbations: Fill-terrace formation and sediment-signal disruption. *Earth*
1212 *Surface Dynamics* 7, 609–631. <https://doi.org/10.5194/esurf-7-609-2019>, 2019.
- 1213 Tofelde, S., Schildgen, T.F., Savi, S., Pingel, H., Wickert, A.D., Bookhagen, B., Wittmann, H., Alonso,
1214 R.N., Cottle, J., Strecker, M.R. 100 kyr fluvial cut-and-fill terrace cycles since the Middle
1215 Pleistocene in the southern Central Andes, NW Argentina. *Earth and Planetary Science Letters*
1216 473, 141–153. <https://doi.org/10.1016/j.epsl.2017.06.001>, 2017.
- 1217 Uppala, S.M., Kållberg, P.W., Simmons, A.J., Andrae, U., Bechtold, V.D.C., Fiorino, M., Gibson, J.K.,
1218 Haseler, J., Hernandez, A., Kelly, G.A., Li, X., Onogi, K., Saarinen, S., Sokka, N., Allan, R.P.,
1219 Andersson, E., Arpe, K., Balmaseda, M.A., Beljaars, A.C.M., Berg, L., Van De, Bidlot, J.,
1220 Bormann, N., Caires, S., Chevallier, F., Dethof, A., Dragosavac, M., Fisher, M., Fuentes, M.,
1221 Hagemann, S., Hólm, E., Hoskins, B.J., Isaksen, I., Janssen, P.A.E.M., Jenne, R., McNally,
1222 A.P., Mahfouf, J.-F., Morcrette, J.-J., Rayner, N.A., Saunders, R.W., Simon, P., Sterl, A.,
1223 Trenberth, K.E., Untch, A., Vasiljevic, D., Viterbo, P., Woollen, J. The ERA-40 re-analysis.
1224 *Quarterly Journal of the Royal Meteorological Society* 131, 2961–3012.
1225 <https://doi.org/10.1256/qj.04.176>, 2005.



- 1226 Valla, P.G., Shuster, D.L., Van Der Beek, P.A. Significant increase in relief of the European Alps during
1227 mid-Pleistocene glaciations. *Nature Geoscience*, 4(10), 688–692.
1228 <https://doi.org/10.1038/ngeo1242>, 2011.
- 1229 van den Berg, van Saparoea, A.-P. H., Postma, G. Control of climate change on the yield of river
1230 systems, Recent Adv. Model. Siliciclastic Shallow-Marine Stratigr. SEPM Spec. Publ., 90, 15–
1231 33, 2008, <https://doi.org/10.2110/pec.08.90.0015>
- 1232 Ventra, D., Nichols, G.J. Autogenic dynamics of alluvial fans in endorheic basins: outcrop examples
1233 and stratigraphic significance. *Sedimentology*, 61(3), 767–791.
1234 <https://doi.org/10.1111/sed.12077>, 2014.
- 1235 Vera, C., Higgins, W., Amador, J., Ambrizzi, T., Garreaud, R., Gochis, D., Gutzler, D., Lettenmaier,
1236 D., Marengo, J., Mechoso, C.R., Nogues-Paegle, J. Toward a unified view of the American
1237 monsoon systems. *Journal of Climate*, 19(20), 4977–5000. <https://doi.org/10.1175/JCLI3896.1>,
1238 2006.
- 1239 Vezzoli, L., Acocella, V., Omarini, R., Mazzuoli, R. Miocene sedimentation, volcanism and
1240 deformation in the Eastern Cordillera (24°30' S, NW Argentina): Tracking the evolution of the
1241 foreland basin of the Central Andes. *Basin Research* 24, 637–663.
1242 <https://doi.org/10.1111/j.1365-2117.2012.00547.x>, 2012.
- 1243 Vizey, E.K., Cook, K.H. Relationship between Amazon and high Andes rainfall. *Journal of Geophysical*
1244 *Research: Atmospheres*, 112(D7). <https://doi.org/10.1029/2006JD007980>, 2007.
- 1245 von Blanckenburg, F. Cosmogenic nuclide evidence for low weathering and denudation in the wet,
1246 tropical highlands of Sri Lanka. *Journal of Geophysical Research: Earth Surface*, 109, F03008.
1247 <https://doi.org/10.1029/2003JF000049>, 2004.
- 1248 Wang, X., Auler, A.S., Edwards, R.L., Cheng, H., Ito, E., Wang, Y., Kong, X., Solheid, M. Millennial-
1249 scale precipitation changes in southern Brazil over the past 90,000 years. *Geophysical Research*
1250 *Letters* 34 (23). <https://doi.org/10.1029/2007GL031149>, 2007.
- 1251 Wickert, A.D., Schildgen, T.F. Long-profile evolution of transport-limited gravel-bed rivers. *Earth*
1252 *Surface Dynamics*, 7(1), 17–43. <https://doi.org/10.5194/esurf-7-17-2019>, 2019.
- 1253 Wittmann, H., Malusà, M.G., Resentini, A., Garzanti, E., Niedermann, S. The cosmogenic record of
1254 mountain erosion transmitted across a foreland basin: Source-to-sink analysis of in situ ¹⁰Be,
1255 ²⁶Al and ²¹Ne in sediment of the Po river catchment. *Earth and Planetary Science Letters* 452,
1256 258–271. <https://doi.org/10.1016/j.epsl.2016.07.017>, 2016.
- 1257 Zech, J., Terrizzano, C.M., Garcia Morabito, E., Veit, H., Zech, R. Timing and extent of late Pleistocene
1258 glaciation in the arid Central Andes of Argentina and Chile (22°–41°S). *CIG* 43(2):697–
1259 718. <http://dx.doi.org/10.18172/cig.3235>, 2017.
- 1260 Zondervan, J.R., Stokes, M., Boulton, S.J., Telfer, M.W., Mather, A.E. Rock strength and structural
1261 controls on fluvial erodibility: Implications for drainage divide mobility in a collisional
1262 mountain belt. *Earth and Planetary Science Letters*, 538, 116221.
1263 <https://doi.org/10.1016/j.epsl.2020.116221>, 2020.
- 1264